Geochemistry Geophysics Geosystems G3
AN ELECTRONIC JOURNAL OF THE EARTH SCIENCES
Published by AGU and the Geochemical Society

Article
Volume 10, Number 11
5 November 2009
Q11003, doi:10.1029/2009GC002518
ISSN: 1525-2027

Methane sources feeding cold seeps on the shelf and upper continental slope off central Oregon, USA

Marta E. Torres
College of Oceanic and Atmospheric Sciences, Oregon State University, Corvallis, Oregon 97331, USA (mtorres@coas.oregonstate.edu)

Robert W. Embley
Pacific Marine Environmental Laboratory, NOAA, 2115 Southeast OSU Drive, Newport, Oregon 97365, USA

Susan G. Merle
CIMRS, Oregon State University, 2115 Southeast OSU Drive, Newport, Oregon 97365, USA

Anne M. Tréhu and Robert W. Collier
College of Oceanic and Atmospheric Sciences, Oregon State University, Corvallis, Oregon 97331, USA

Erwin Suess
College of Oceanic and Atmospheric Sciences, Oregon State University, Corvallis, Oregon 97331, USA

Also at Leibniz Institute of Marine Sciences at University of Kiel (IFM-GEOMAR), D-24148 Kiel, Germany

Also at Marine Research Consortium, D-10117 Berlin, Germany

Katja U. Heeschen
National Oceanography Centre, Southampton, University of Southampton, Southampton SO14 3ZH, UK

[1] We report on a bathymetric mapping and remotely operated vehicle surveys along the 100–600 m region offshore Oregon from 43°50′N to 44°18′N. We interpret our results in light of available geophysical data, published geotectonic models, and analogous observations of fluid venting and carbonate deposition from 44°30′N to 45°00′N. The methane seepage is defined by juxtaposition of a young prism, where methane is generated by bacterial activity and its release is modulated by gas hydrate dynamics, against older sequences that serve as a source of thermogenic hydrocarbons that vent in the shelf. We hypothesize that collision of a buried ridge with the Siletz Terrane results in uplift of gas hydrate bearing sediments in the oncoming plate and that the resulting decrease in pressure leads to gas hydrate dissociation and methane exolution, which, in turn, may facilitate slope failure. Oxidation of the released methane results in precipitation of carbonates that are imaged as high backscatter along a 550 ± 60 m benthic corridor.

Components: 11,611 words, 8 figures, 3 tables.

Keywords: seep carbonates; Heceta Bank; gas hydrate; methane seeps; Cascadia margin.

Index Terms: 3002 Marine Geology and Geophysics: Continental shelf and slope processes (4219); 3045 Marine Geology and Geophysics: Seafloor morphology, geology, and geophysics; 1051 Geochemistry: Sedimentary geochemistry.

Received 25 March 2009; **Revised** 17 August 2009; **Accepted** 28 August 2009; **Published** 5 November 2009.

Torres, M. E., R. W. Embley, S. G. Merle, A. M. Tréhu, R. W. Collier, E. Suess, and K. U. Heeschen (2009), Methane sources feeding cold seeps on the shelf and upper continental slope off central Oregon, USA, *Geochem. Geophys. Geosyst.*, *10*, Q11003, doi:10.1029/2009GC002518.

1. Introduction

[2] Natural gas seeps are now known to be widely distributed along passive, convergent and transform margins worldwide. They range from micro to macroseepages [e.g., *Hornafius et al.*, 1999]; and include release from primarily biogenic and thermogenic gas reservoirs [e.g., *Sassen et al.*, 2001; *Kvenvolden and Lorenson*, 2001] as well as from decomposition of methane hydrates [e.g., *Suess et al.*, 1999]. These seeps are usually discovered through the biological communities they support, as well as by direct observations of gas bubbles, oil slicks, and mineral deposits. Geologic reservoirs on the seafloor are thought to contribute from 5 to 10% of the current global atmospheric input and constitute a significant fraction of global methane discharge inventories [e.g., *Milkov et al.*, 2003; *Etiope and Milkov*, 2004].

[3] Microbial and thermogenic sources feed methane to the bottom water and generate distinct signatures within the water column. These two sources have been documented along the northeast Pacific margin from northern California to Canada (Figure 1), and have been recognized by extensive hydrographic surveys offshore Oregon [*Heeschen et al.*, 2005]. Authigenic carbonates associated with cold methane seeps form as the result of a complex interplay of microbial and hydrological processes and serve as valuable tools for fingerprinting the carbon source [*Luff et al.*, 2004].

[4] At the Oregon-Washington margin, the presence of authigenic carbonates along the shelf and accretionary prism was first reported in the 1980s [e.g., *Kulm et al.*, 1986; *Pearcy et al.*, 1989; *Kulm and Suess*, 1990]. More recent work on carbonate samples from this margin highlights the roles of gas hydrate destabilization and anaerobic oxidation of methane in carbonate formation [e.g., *Bohrmann et al.*, 1998; *Greinert et al.*, 2002; *Luff et al.*, 2004; *Teichert et al.*, 2005a, 2005b]. The bulk of seep and carbonate analyses has focused on environments that occur at water depths greater than 600 m, well within the pressure and temperature conditions that define the gas hydrate stability zone [*Dickens and Quinby-Hunt*, 1994].

[5] There is however, a growing interest to understand the processes that regulate methane hydrate dynamics and associated gas release at water depths that correspond to the upper limit of gas hydrate stability. Release of free gas has been observed at locations where a bottom simulating reflector (BSR) appears to pinch out at or near the seafloor, at water depths consistent with thermodynamic predictions of gas hydrate stability [e.g., *Pecher et al.*, 1998, 2005; *Rao et al.*, 2002]. Gas hydrate stability in depth horizon is particularly susceptible to pressure and temperature changes caused by global climate change [*Kennett et al.*, 2003; *Vogt and Jung*, 2002; *Maslin et al.*, 2004]. Destabilization of this zone has been invoked in slope stability studies in the Norwegian margin [e.g., *Mienert et al.*, 2005; *Sultan et al.*, 2004] and offshore New Zealand [*Pecher et al.*, 2005]. This process has also been associated with widespread slumping of continental margins in the Pleistocene [e.g., *Dillon and Paull*, 1983], and may result in significant methane input to the atmosphere [*Beget and Addison*, 2007].

[6] Here we present carbonate and geophysical data from the upper continental slope off Oregon, which reveal the presence of localized zones of biogenic methane discharge from approximately 43°N to 45°N, a region that corresponds to the location of a basaltic ridge buried beneath a thick accretionary complex [*Fleming and Tréhu*, 1999]. We postulate a scenario where tectonic controls, specifically sediment uplift due to subduction of a basaltic ridge, leads to gas hydrate destabilization in this margin. Earthquake activity in this area is known to play a major role on the generation of seafloor slumping, which, in turn, may trigger gas hydrate dissociation [*Goldfinger et al.*, 2000]. Our attempt to relate the geochemical data to recent tectonic uplift that may trigger gas exolution, further illustrates the complex interactions between tectonics, fluid flow and methane discharge in this and other active margins worldwide.

[7] Destabilization of gas hydrate deposits at the depth where the seafloor intersects the gas hydrates stability boundary results in methane discharge along the 550 ± 60 m benthic corridor and in the formation of seep carbonates with a gas hydrate

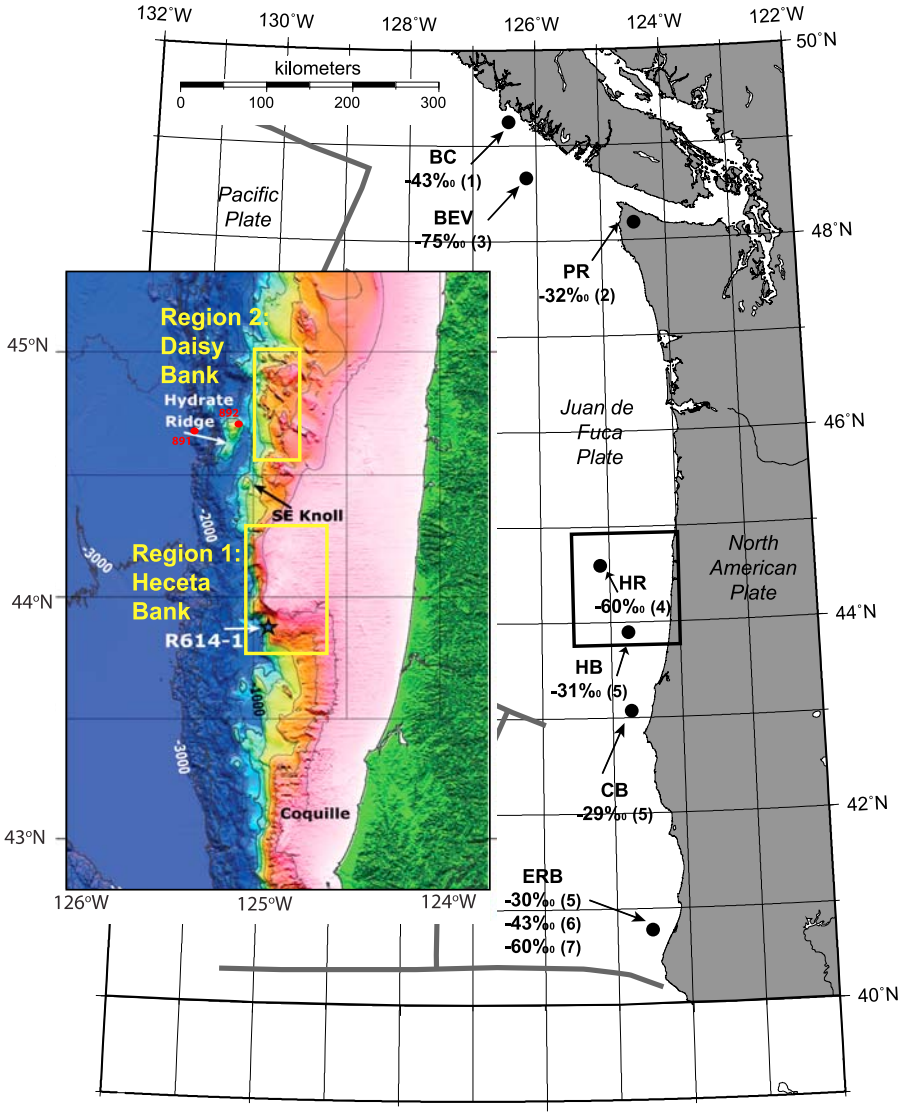

Figure 1. Location of the study area within the tectonic context of the region. Closed circles designate seeps where the isotopic composition of the discharging methane has been reported, shown here as ‰ PDB. BC, Barkley Canyon; BEV, Bulls Eye Vent; PR, Pysht River; HR, Hydrate Ridge; HB, Heceta Bank; CB, Coos Bay; ERB, Eel River Basin. Data sources are as follows: 1, *Pohlman et al.* [2005]; 2, *Riedel et al.* [2006]; 3, *Snavely* [1987]; 4, *Suess et al.* [1999]; 5, *Collier and Lilley* [2005]; 6, *Kvenvolden and Field* [1981]; 7, *Brooks et al.* [1991]. Inset shows locations of the two regions targeted in this study on a bathymetric map. Sites 891 and 892 are also shown.

isotopic fingerprint. Juxtaposed to this biogenic carbon source, thermogenic gases are released at seeps located in the shelf [*Collier and Lilley*, 2005] and constitute a significant methane source to the water column [*Heeschen et al.*, 2005]. These shelf seeps generate pockmarks and carbonate deposits that are imaged in seafloor sonar surveys.

2. Geologic Setting

[8] Heceta Bank and other major banks on the Oregon outer shelf are composed of late Miocene and Pliocene sedimentary rocks that rise above surrounding Pleistocene sediment, and are likely to be fault controlled [*Kulm and Fowler*, 1974]. These central Cascadia banks are thought to have been part of a continuous Cenozoic fore-arc basin that extended from Eel River Basin to offshore Vancouver Island. *Fleming and Tréhu* [1999] describe the discrete banks along the central Oregon shelf as generated by the transfer of seamounts from the subducting to the overlying plate. They document the presence of a N–S trending ridge buried beneath the accretionary complex from

about 43°N to 45°N, and suggest that this mafic structure was formed by the obduction of several seamounts over the past several million years.

[9] Farther offshore, the lower continental slope is composed of folded and faulted abyssal plain turbidites and hemipelagic sediments that have been accreted to the margin since the early Pleistocene (~1.7–1.6 Ma) [*Johnson et al.*, 2006; *Chevallier et al.*, 2006] and comprise the modern Cascadia accretionary wedge [*Kulm and Fowler*, 1974]. Much of the 3–4 km thick sediment cover of the subducting plate has accreted since, either by offscraping at the deformation front or by underplating beneath the accretionary complex some tens of kilometers east of the deformation front [*MacKay et al.*, 1992; *MacKay*, 1995]. Microbial methane production occurs primarily in the upper 100 m, and began when these sediments were part of the incoming plate that underlay approximately 3 km of water [*Claypool et al.*, 2006]. The methane-bearing sediments have since undergone significant uplift by incorporation onto the accretionary margin, which leads to a significant decrease in methane solubility and subsequent gas exolution [*Claypool et al.*, 2006]. The accumulating gas phase undergoes buoyant migration toward the seafloor by finding or creating permeable channels [*Tréhu et al.*, 2004] and is manifested by gas seepage and gas hydrate formation on the Cascadia margin [*Torres et al.*, 2004; *Tréhu et al.*, 2006].

3. Methods

3.1. Bathymetric and Seafloor Surveys

[10] A high-resolution bathymetric survey of Heceta Bank was conducted from the R/V *Ocean Alert* using a Simrad EM300 (30 kHz) sonar system (region 1, inset in Figure 1). Survey lines were run at an average speed of 10 knots with swath widths averaging about three times the water depth. Differential GPS navigation provided positional accuracy of <5 m, about equal to the optimal grid cell size used in generating the bathymetry and backscatter maps at the shallowest depths of the bank (Figure 2).

[11] The data were postprocessed on board using the SWATHED software package. The postprocessing removed obvious bad data points, corrected for tidal effects and refraction of the raypaths, and gridded the data. Sound velocity corrections were made using a series of hydrocasts in this area. The EM300 system produces a high-quality backscatter data set from which we derived a high aspect ratio side scan image of the seafloor that is precisely referenced with the bathymetry data [*Hughes-Clarke et al.*, 1996].

[12] A series of dives with the remotely operated vehicle ROPOS were conducted in 2000 and 2001 to ground truth various topographic and textural boundaries on the EM 300 map. The locations of these dives are superimposed on the topography and acoustic backscatter in Figure 2. The ROPOS was navigated by an ultrashort baseline Trackpoint II system across real-time displays of the side-lit bathymetry and backscatter. A three-chip color camera and a black and white SIT camera were recording continuously during the dives and a mounted laser system provided scale for the three-chip camera.

[13] To complement these data, we draw on available surveys and samples from Daisy Bank region (region 2, inset in Figure 1). Bathymetry and side-scan sonar data are from *Johnson et al.* [2003] and *Lanier et al.* [2007]; seismic, gravity and magnetic data surveys are from *Tréhu et al.* [1995] and *Fleming and Tréhu* [1999]; seafloor observations and carbonates along 45°N were collected by TV-guided sampling following a video sled survey by OFOS (Ocean Seafloor Observation System) during the R/V *Sonne* Cruise SO143 [*Bohrmann et al.*, 2000]; water column data are from *Heeschen et al.* [2005]; and near-bottom water samples in the upper slope region were collected with the WHOI TowCam sled (http://www.whoi.edu/instruments/viewInstrument.do?id = 9929).

3.2. Carbonate and Water Samples

[14] Carbonate samples were retrieved from active seeps along the Heceta shelf and slope during ROPOS dives. In addition, two samples previously collected from seep sites on the upper slope at ~45°N are included in this study [*Bohrmann et al.*, 2000]. Sample locations are listed in Table 1.

[15] Subsamples for geochemical characterization were taken from slab surfaces using a handheld microdrill. The sample mineralogy was determined by XRD (X-ray diffraction) analysis using a Philips XRG 3100 at the Willamette Geological Service, OR. Isotopic characterization was conducted in subsamples collected along transects drilled on the carbonate specimens, as shown in Figure 3. The carbonate powders were reacted with 100% phosphoric acid at 75°C in an online carbonate preparation line (Kiel-II device) connected to a Finnigan MAT 252 mass spectrometer, at Oregon

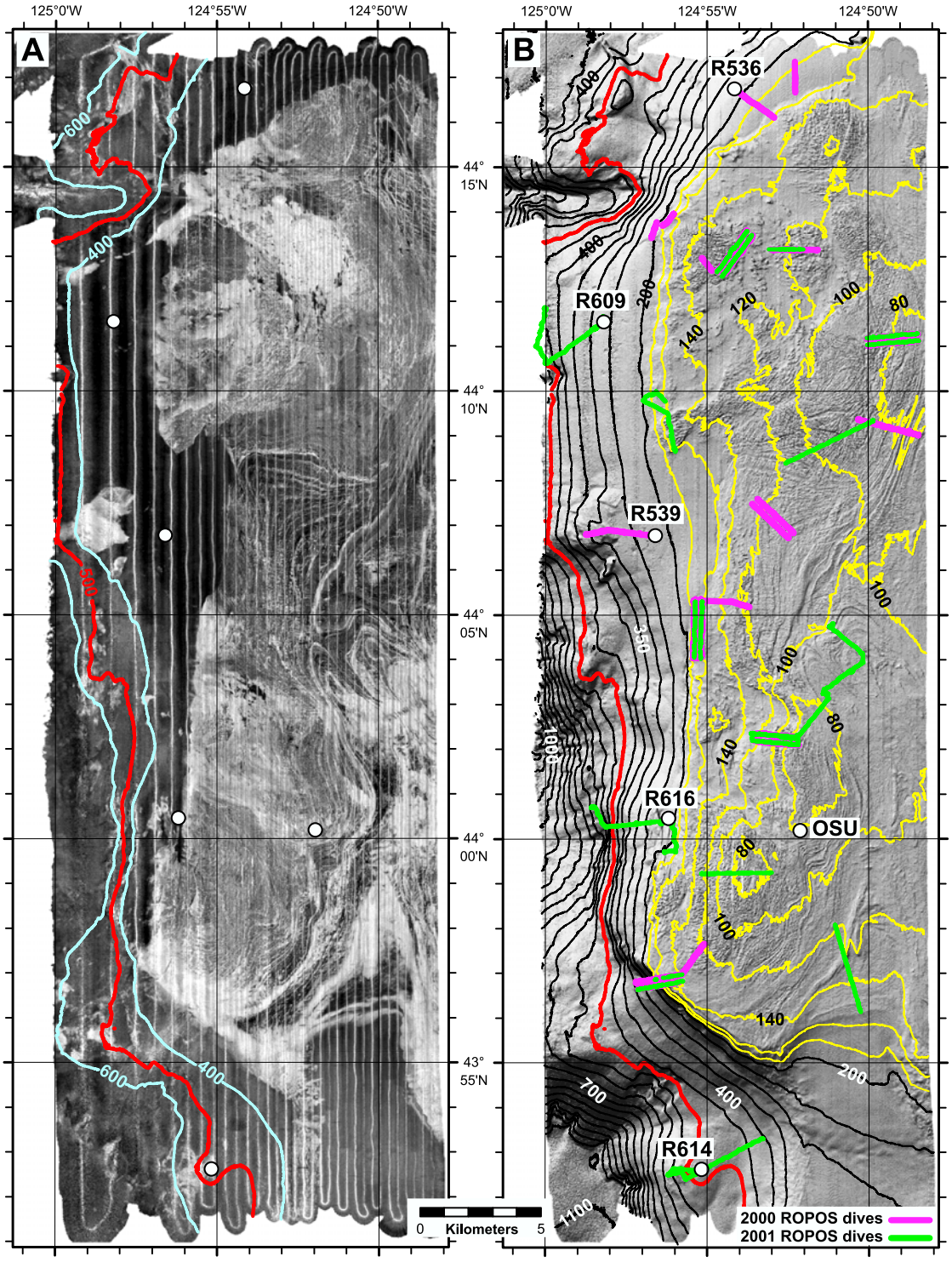

Figure 2. (a) EM300 high-resolution acoustic reflectivity (backscatter) data at Heceta Bank. Bright implies high return. Grid cell size is 10 m. We propose that areas of high reflectivity along the 400 to 600 m corridor (inside light blue contours) correspond to carbonate deposition at sites of methane discharge. The 500 m contour is indicated by bold red lines in both Figures 2a and 2b, as it demarks the approximate upper limit of gas hydrate stability in this margin. Location of carbonate samples is indicated by white circles in both Figures 2a and 2b. (b) EM300 high-resolution bathymetry shaded relief. Grid cell size is 10 m. Illumination is from the west. Bathymetric depths range from 65 m at the top of the bank to 1160 m at the southwest edge of the survey. Contour intervals vary, with 20 m contours (yellow) extending out to 180 m depth and 50 m contours (black) at depths of 200 m and deeper. Carbonate sample names are indicated, as well as ROPOS dives in 2000 (magenta) and 2001 (green).

Table 1. Station Description

Sample	Longitude (°N)	Latitude (°W)	Description	Water Depth (m)
			ROPOS Survey	
R536-5	124.902	44.279	North of the bank. Small pockmark. ~350 m w–e; ~300 m n–s. Bubbles, mat, and biota in the area.	221
R616-7	124.936	44.007	Ridge area just west of the southern bank, ~140 m × 140 m. Bacterial mats.	223
R539-2	124.943	44.112	West of the central bank saddle. Sample from a small pockmark area. ~130 m w–e; ~130 n–s. Small pockmark area. Bubbles, mat, and live biota in the carbonate area.	219
R609-3	124.969	44.192	West of the northern bank. Small pockmark with 2 bright areas ~150 m w–e; 120 m n–s. Some bubbling and bacterial mats in the pockmark area.	275
R614-1	124.919	43.876	Large carbonate area south of the bank. Seepage area is very large, ~2000 m × 2000 m, extending from 490 to 590 m water depth. Abundance of carbonates, bacterial mats, and live clam colonies.	493
			TV-Guided Grab Samples[a]	
TVG 49-1	124.836	44.836	Carbonate chimney. Many nonseep organisms.	344
TVG167-1	124.838	44.847	High-backscatter area corresponding to the location where the BSR is observed to outcrops on the seismic records. Carbonate and vesicomyid clams.	567
			TowCam Surveys (TC)	
TC-1	125.000	44.217	High-backscatter area in the location where a BSR is observed in the seismic data to outcrop. Extensive carbonates, some clam colonies, and few patches of bacterial mats.	475–600
TC-6	124.883	44.733	Carbonate deposits a few clam patches.	450–601
TC-7	124.897	44.558	Carbonate deposits.	500–600
			Hydrocast Stations	
NH-28	124.883	44.732	From *Heeschen et al.* [2005].	
NH-30	124.957	44.841	From *Heeschen et al.* [2005].	
NH-45	124.917	44.533	From *Heeschen et al.* [2005].	
SO143-120	124.963	44.837	From *Heeschen et al.* [2005].	
CTD-10	124.981	44.281	This study.	633

[a] From *Bohrmann et al.* [2000].

State University, College of Oceanic and Atmospheric Science (COAS-OSU). Precision of the analysis is better than ±0.03‰ and 0.07‰ for δ^{13}C and δ^{18} O, respectively. All isotopic values are reported relative to PDB. A subset of these carbonate powders was acid digested and analyzed for their chemical composition by Inductively Coupled Plasma Optical Emission Spectroscopy (ICP-OES) at the W. M. Keck Collaboratory in COAS-OSU.

[16] Water column samples were collected on a cruise of opportunity in 2008 to document the methane concentration seaward of Heceta Bank. In addition several samples were obtained from TowCam surveys of the upper slope region, targeting areas of high-reflectivity zones in the side-scan sonar data, along the 400 to 600 m benthic corridor. Samples were analyzed for their methane content using a purge and trap technique modified from *Popp et al.* [1995]. The location of these stations is listed in Table 1 and the methane concentration is shown in Table 2.

4. Results and Discussion

4.1. Geologic Mapping

[17] Using the bathymetry and backscatter imagery (Figure 2) we compiled a composite map of the Heceta Bank region (Figure 4), which includes location of bedding planes, faults and pockmarks. On the basis of available core data, the Miocene-Pliocene boundary is also shown.

[18] The backscatter patterns we observe on Heceta Bank are complex and reflect a long history of uplift, erosion, deposition and eustatic sea level change. The edge of the bank is marked by an

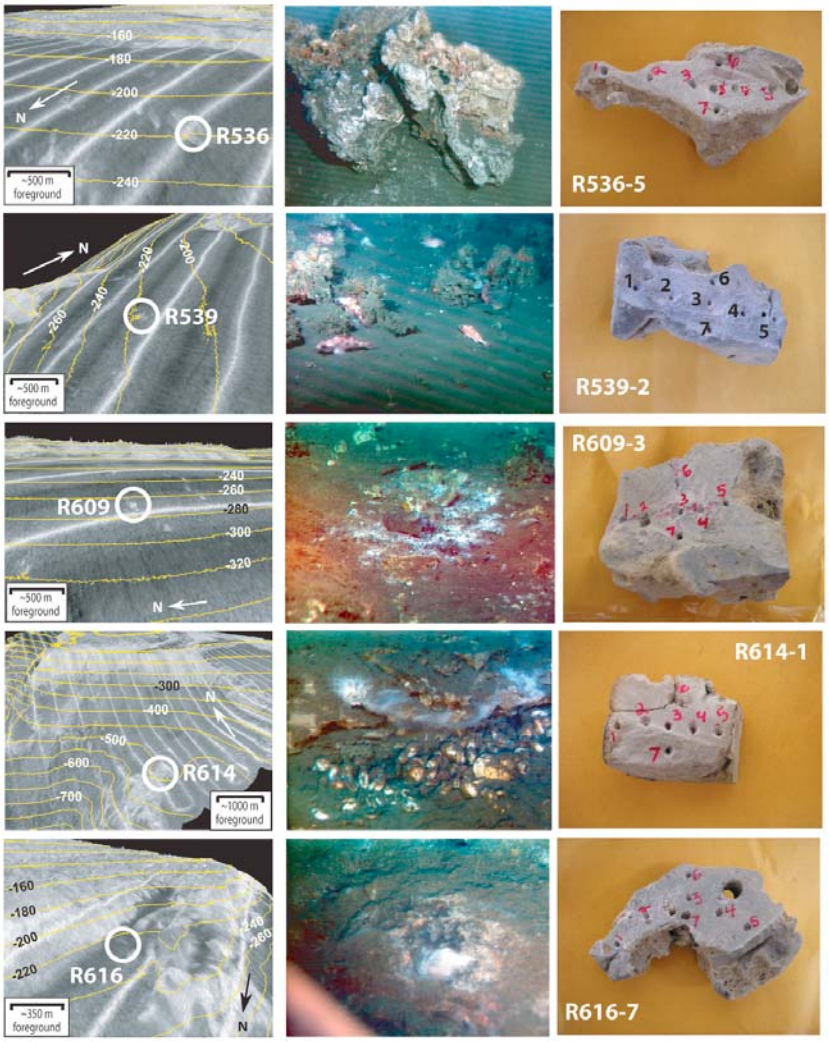

Figure 3. (left) EM300 acoustic backscatter data overlain on 10 m bathymetry at each of the ROPOS dive sites where carbonate samples were recovered. EM300 data are vertically exaggerated 10 times. (middle) Images of each sample site, featuring carbonates, bacterial mat, bivalves, and rockfish. (right) Carbonate specimens analyzed and location of subsamples collected. Sample site descriptions are listed in Table 1. Data obtained from these samples are listed in Table 3.

abrupt change from high to low backscatter, which in several places is accompanied by a small scarp or bench that has been interpreted to be the downwarped 18 Ka shoreline. At Heceta Bank, folds, faults and several different joint sets, are easily mapped in outcrops developed by differential erosion. The eroded planes appear to be primarily outcrops of early Pliocene age, with only two late Miocene samples recovered from the northwestern section of the bank [*Muehlberg*, 1971]. Small scarps on the central and southern bank are interpreted as recent faults, whereas a cluster of east facing, small curvilinear scarps on the southwestern corner of the bank may be related to the Heceta megaslide, dated at 110 ka. The slide headwall has been mapped just seaward of the western flank of Heceta Bank [*Goldfinger et al.*, 2000]. The slide scars on the southwestern portion of the survey area may represent continued mass wasting of the headwall.

4.2. Seep Structure Types

[19] Dives with ROPOS on Heceta Bank and its seaward upper slope discovered methane seeps in water depths ranging from <100 to 600 m (Figures 3 and 4). The seeps occur in four geologic settings.

[20] Type I is characterized by distinct "pockmarks" just seaward of the bank in water depths between 150 and 400 m. More than 20 of these small but well-defined depressions were distin-

Table 2. Methane Concentration in Water Samples Collected Over High-Backscatter Areas During TowCam Dives and From Hydrocast Station CTD-10[a]

Station	Sample	Water Depth (m)	Methane (nmol L^{-1})
TC-1	1	578	13.9
	2	599	14.6
	3	531	13.6
	4	473	24.1
	5	478	26.5
TC-6	2-1	505	44.6
	2-2	451	43.0
	3	558	54.2
	8	601	21.8
	9-1	572	36.3
	9-2	530	21.6
	9-3	500	18.8
	wc-1[b]	300	7.8
	wc-2[b]	250	8.0
TC-7	1	600	15.1
	2	590	17.2
	3	577	34.6
	4	550	23.7
	5	530	37.2
	6	500	48.3
	wc[b]	250	13.0
CTD-10	1	629	11.8
	2	580	18.1
	3	550	34.3
	4	525	39.4
	5	500	20.7
	6	450	13.7
	7	400	22.4
	8	300	19.1
	9	200	12.6
	10	100	11.4
	11	0	6.4

[a] TC, TowCam.
[b] Water column samples collected with the TowCam on the way back to the surface are designated with wc; all other samples were collected with the TowCam less than 4 m from the seafloor.

guished on the EM300 imagery by their relatively high-backscatter signal. The pockmarks are circular features of 100–200 m in diameter and have up to 15 m of relief. Many have a slightly raised center. Three northern sites were visited on Dive R536, two sites on the northwestern side on Dive R609 and one site on the western side on Dive R539 (Figures 2 and 3). All visited pockmarks had carbonate deposits and most show evidence of present-day activity in the form of microbial mats, chemosynthetic fauna and bubble emissions. Several *Solemya* sp. valves and one live specimen of the thyasirid bivalve *Conchocele bisecta* (A. Valdes, personal communication, 2000) were recovered from these seeps.

[21] In type II seeps, gas is discharged directly out of the outcropping rock on the shallow part of the bank. There are several of these type II seeps characterized by gas bubble streams at the top of Heceta Bank in less than 100 m of water. *Collier and Lilley* [2005] describe one such site in detail and showed that these seeps tap thermogenic gas reservoirs. Type II seeps are probably controlled by fracture permeability in the underlying bedrock but they do not seem to be associated with any particular structural lineations. There is no significant sediment cover at these seeps nor are there any carbonate concretions at these locations. Rapid venting of gas from the bedrock to the water column precludes any anaerobic oxidation of methane needed for carbonate formation.

[22] Type III seep has a well-defined underlying structural control. The only surveyed seep of this type is a 100-m-long low ridge trending NW–SE (~110°) at the SW corner of the bank (Dive R616, Figure 2). The ridge is covered with patches of bacterial mats. It is plated with carbonates lying at roughly 90 degrees to the trend of the ridge, aligning with the regional NW–SE left-lateral strike slip faults along the Cascadia margin [*Goldfinger et al.*, 1992, 1997]. This suggests that the precipitating fluids are indeed migrating through structurally controlled pathways.

[23] Type IV is a large (~4 km^2) area of acoustically reflective seafloor located south of Heceta Bank in the depth range of 490 to 590 m. Active venting over much of the area is evidenced by carbonate deposition, microbial mats, and live aggregations of the bivalve *Calyptogena pacifica*.

4.3. Authigenic Carbonate Formation

[24] Authigenic carbonates, a common feature at methane seep sites, are known to provide critical data on fluid sources and carbon cycling processes. Extensive reviews of modern and ancient seep carbonates, and their relationship to diagenetic, hydrologic, geochemical and microbiological processes are provided by *Campbell et al.* [2002], *Boetius and Suess* [2004], *Campbell* [2006], and *Jørgensen and Boetius* [2007]. Microbially generated methane is produced as an end product of the metabolism of a diverse group of obligate anaerobic archaea, generally known as methanogens [e.g., *Hinrichs et al.*, 1999; *Colwell et al.*, 2008]. This reaction results in the production of isotopically light biogenic methane and a residual dissolved inorganic carbon (DIC) enriched in ^{13}C. Anaerobic oxidation of methane (AOM [*Boetius et al.*, 2000;

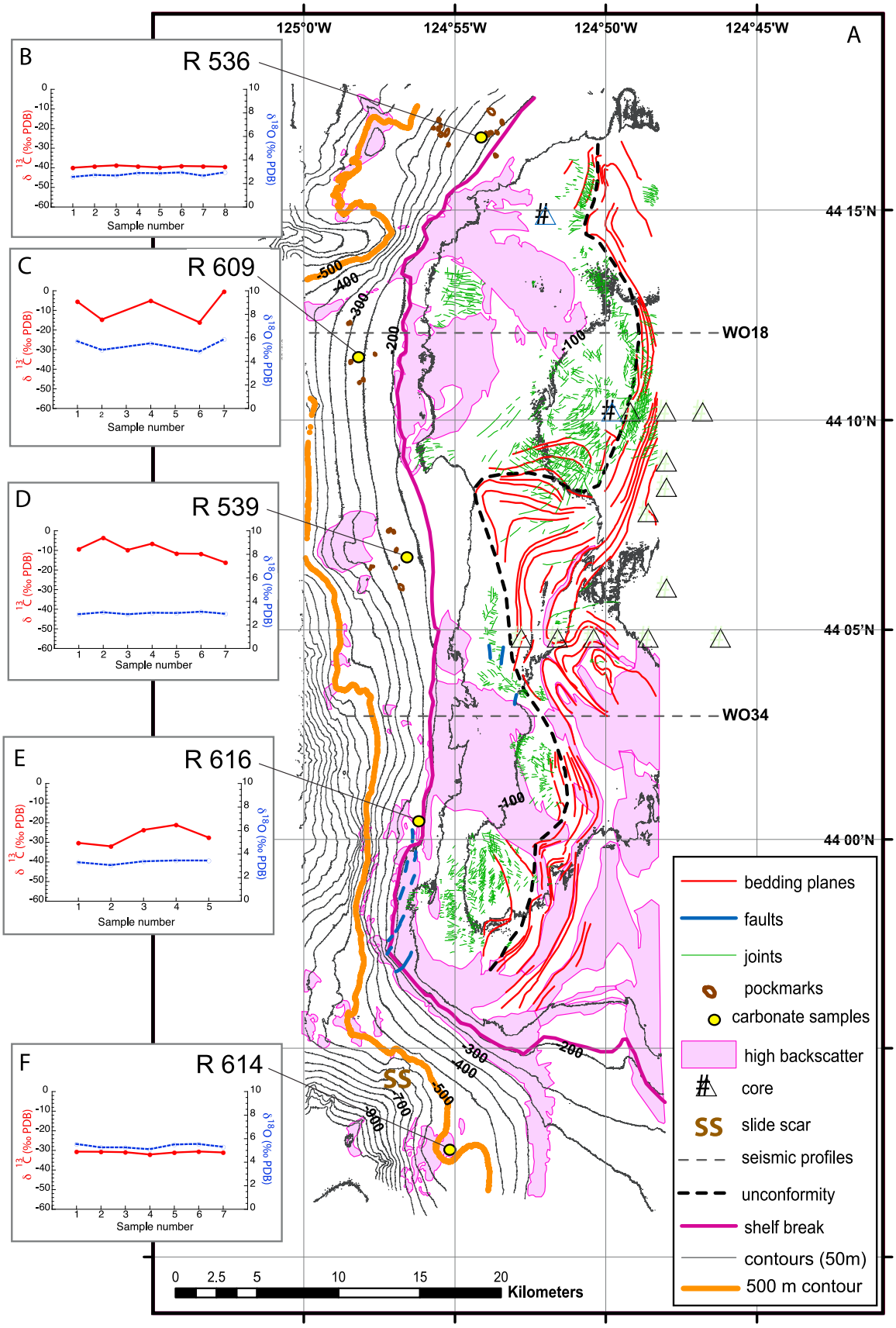
A
B
R 536
C
R 609
D
R 539
E
R 616
F
R 614
Sample number
δ 13C (‰ PDB)
δ18O (‰ PDB)
125°0'W
124°55'W
124°50'W
124°45'W
44 15'N
44 10'N
44 05'N
44 00'N
WO18
WO34
-500
-400
-300
-200
-100
-700
-900
SS
0 2.5 5 10 15 20
Kilometers
bedding planes
faults
joints
pockmarks
carbonate samples
high backscatter
core
slide scar
seismic profiles
unconformity
shelf break
contours (50m)
500 m contour

Figure 4

Hinrichs et al., 1999]) depleted in ^{13}C generates light DIC. Distinct dissolved inorganic carbon pools with light ($\delta^{13}C < -45‰$ [*Torres et al.*, 2003]) and heavy ($\delta^{13}C$ from + 5‰ to +30‰ [*Torres and Kastner*, 2009]) isotopic signatures have been reported in pore fluids of the Cascadia accretionary margin. These distinct inorganic carbon reservoirs generate carbonate deposits with distinct isotopic fingerprints. Light ($\delta^{13}C$ −20‰ to −50‰) carbonates resulting form oxidation of biogenic methane are well documented at methane seeps on Hydrate Ridge [e.g., *Teichert et al.*, 2005a, 2005b; *Greinert et al.*, 2002]. In contrast, the heavy ($\delta^{13}C$ −2‰ to +26‰) carbonates recovered offshore Oregon, along a vertical fault zone in the Daisy Bank region (Figure 1), reflect precipitation form residual DIC [*Sample et al.*, 1993].

[25] The thermal alteration of organic matter generates isotopically heavier methane and higher-order hydrocarbons. Biogenic and thermogenic gases can usually be distinguished on the basis of chemical and isotopic composition. Thus, whereas carbonates with low $\delta^{13}C$ values clearly reflect oxidation of microbial methane; high $\delta^{13}C$ values can reflect either a thermogenic methane source or carbonate precipitation from a heavy residual DIC [*Claypool and Kaplan*, 1974].

[26] The oxygen isotopic composition of deep-seated fluids shows a range of values, which reflect deep fluid sources and diagenetic reactions. In particular, clay dehydration in accretionary margins leads to fluids enriched in ^{18}O [*Dählmann and de Lange*, 2003]. Although significant fluid freshening in the Cascadia margin has been attributed to clay dehydration reactions [*Torres et al.*, 2004], the oxygen isotopic composition of these fluids is highly depleted in ^{18}O because of an interplay of diagenetic reactions that overprint the clay dehydration signal [*Tomaru et al.*, 2006]. The isotopic composition of carbonate samples recovered from ODP Site 891 are indeed depleted in ^{18}O ($\delta^{18}O$ = −16.5‰ to −6.2‰), and a sample recovered from a fault zone at ODP Site 892 is also depleted in ^{18}O ($\delta^{18}O$ = −16.5‰), providing evidence for migration of deep seated fluids through this horizon [*Sample and Kopf*, 1995]. Similarly, the $\delta^{18}O$ values of the Daisy Bank carbonates (−12.7 to −6.4‰) indicate precipitation from highly depleted $\delta^{18}O_{pore}$ fluids and high temperatures, consistent with a heavy residual carbon in the dissolved inorganic pool as the source for the carbonate [*Sample and Reid*, 1998]. Thus, in the Cascadia margin, carbonates associated with fluid migration from deep sources have heavy carbon and light oxygen isotopic values.

4.4. Thermogenic Carbon Source

[27] Aragonite samples recovered from types I and III seeps (<300 m water depth, Tables 1 and 3), reveal formation at seafloor seep sites. *Luff et al.* [2004] have shown that although the chemical composition of precipitating fluids at methane seeps may favor calcite formation, aragonite is commonly observed at these sites, where it appears to be induced and catalyzed by microbial communities involved in AOM.

[28] The oxygen isotopic composition of these aragonite samples range from 2.54 to 3.44‰ PDB (Table 3 and Figure 5a). Assuming water temperatures of 7°C at the present seep depth of ~200 m, the isotopic composition of the water from which these deposits formed can be estimated using well established relationships [e.g., *Böhm et al.*, 2000; *Hudson and Anderson*, 1989]. The range of measured $\delta^{18}O_{aragonite}$ values reflects precipitation in equilibrium with the ambient seawater temperatures that deviates from the present $\delta^{18}O_{seawater}$ of 0.08‰ by ±0.43‰ SMOW. If we use the average $\delta^{18}O_{aragonite}$ value of 2.98‰ PDB (Figure 5a), we obtain a $\delta^{18}O_{water}$ of 0.05‰ SMOW, which is very close to the present-day seawater value, supporting precipitation at or near the seafloor.

[29] Except for one seep (R536-5), all carbonates sampled at the shelf region (<300 m depth) are less enriched in ^{12}C than would be expected if they had formed from a biogenic methane pool (Table 3). These data are consistent with carbon isotopic measurements in gas samples collected from the OSU seep on southern Heceta Bank (Figure 2), which revealed that the discharging fluids there are mostly thermogenic methane, with a heavy isotopic composition ranging from −29 to −35‰ [*Collier and Lilley*, 2005]. These heavy hydrocarbons are

Figure 4. (a) Geologic interpretation of Heceta Bank from bathymetric and backscatter imagery including published data available on dated samples (cores demarked with number symbol) and seismic reflection profiles WO18 and WO34 [*Muehlberg*, 1971; *McNeill et al.*, 2000]. Orange line denotes the 500 m bathymetric contour. Location of pockmarks and carbonate samples are also shown. (b–f) The carbon (red solid line) and oxygen (blue dashed line) stable isotope ratios of the carbonate samples.

Table 3. Carbonate Characterization

Sample	$\delta^{13}C$ (‰ PDB)	$\delta^{18}O$ (‰ PDB)	Mineralogy	Mg/Ca (mol %)
			Heceta Bank	
536.5.1	−40.07	2.54	Aragonite, trace Sr-apatite, trace calcite	
536.5.2	−39.36	2.71	Aragonite, trace Sr-apatite, trace calcite	
536.5.3	−38.82	2.66	Aragonite, trace Sr-apatite, trace calcite	
536.5.4	−39.35	2.88	Aragonite, trace Sr-apatite, trace calcite	
536.5.5	−39.91	2.85	Aragonite, trace Sr-apatite, trace calcite	9.4
536.5.6	−39.21	2.93	Aragonite, trace Sr-apatite, trace calcite	
536.5.7	−39.34	2.65	Aragonite, trace Sr-apatite, trace calcite	
536.5.8	−39.58	2.93	Aragonite, trace Sr-apatite, trace calcite	
539.2.1	−9.44	2.90	Aragonite, trace calcite, trace Sr-apatite	4.8
539.2.2	−3.68	3.06	Aragonite, trace calcite, trace Sr-apatite	
539.2.3	−9.90	2.89	Aragonite, trace calcite, trace Sr-apatite	
539.2.4	−6.66	3.02	Aragonite, trace calcite, trace Sr-apatite	
539.2.5	−11.72	3.00	Aragonite, trace calcite, trace Sr-apatite	
539.2.6	−11.82	3.11	Aragonite, trace calcite, trace Sr-apatite	
539.2.7	−16.27	2.93	Aragonite, trace calcite, trace Sr-apatite	
609.3.1	−5.59	5.70	Dolomite	
609.3.2	−14.76	4.96	Dolomite	
609.3.3	2.55	5.92	Dolomite	
609.3.4	−5.17	5.52	Dolomite	
609.3.5	3.06	5.96	Dolomite	
609.3.6	−16.17	4.82	Dolomite	
609.3.7	−0.46	5.86	Dolomite	
614.1.1	−30.71	5.53	Mg-calcite, trace calcite, trace Sr-apatite	
614.1.2	−30.78	5.25	Mg-calcite, trace calcite, trace Sr-apatite	32.0
614.1.3	−30.99	5.24	Mg-calcite, trace calcite, trace Sr-apatite	31.8
614.1.4	−32.17	5.09	Mg-calcite, trace calcite, trace Sr-apatite	27.6
614.1.5	−31.18	5.49	Mg-calcite, trace calcite, trace Sr-apatite	35.0
614.1.6	−30.64	5.53	Mg-calcite, trace calcite, trace Sr-apatite	34.6
614.1.7	−31.15	5.28	Mg-calcite, trace calcite, trace Sr-apatite	32.5
616.7.1	−30.36	3.29	Aragonite, trace Sr apatite, trace Ca-Mg calcite	
616.7.2	−32.12	3.05	Aragonite, trace Sr apatite, trace Ca-Mg calcite	
616.7.4	−23.77	3.37	Aragonite, trace Sr apatite, trace Ca-Mg calcite	
616.7.5	−21.18	3.44	Aragonite, trace Sr apatite, trace Ca-Mg calcite	9.3
616.7.7	−27.62	3.43	Aragonite, trace Sr apatite, trace Ca-Mg calcite	
			Northern Site	
167.1	−30.80	5.05	Mg-calcite, trace calcite	20.9
167.2	−34.88	5.04	Mg-calcite, trace calcite	20.1
167.3	−35.97	4.90	Mg-calcite, trace calcite	19.7
167.4	−36.17	4.96	Mg-calcite, trace calcite	18.8
167.5	−35.54	5.02	Mg-calcite, trace calcite	18.5
49.1	−2.89	6.13	Fe-Mg-Ca carbonate	
49.2	−2.49	6.35	Fe-Mg-Ca carbonate	
49.3	−2.08	6.28	Fe-Mg-Ca carbonate	

likely sourced by Tertiary rocks analogous to those that outcrop in the Olympic Peninsula [*Snavely*, 1987]. The carbonates enriched in ^{13}C thus reflect oxidation of a heavy methane source and precipitation near the seafloor at bottom water temperatures, and are not likely to be the result of upward migration of fluids enriched in heavy DIC.

[30] One of the aragonite samples recovered from a small pockmark in the inner shelf (R536-5, 221 m) has a light carbon isotopic composition indicative of a microbial methane source. This sample indicates gas migration upslope from the modern accreted sediment, but plumbing underneath this feature, and the reason for gas channeling of microbial methane to this shallow seep is not presently understood. Nonetheless, this sample shows that at Heceta Bank both methane sources occur in close proximity to each other.

4.5. Gas Hydrate Dynamics and Microbial Methane Discharge

[31] The sample recovered at the deeper type IV site R614-1 (493 m) is Mg-calcite, and has an

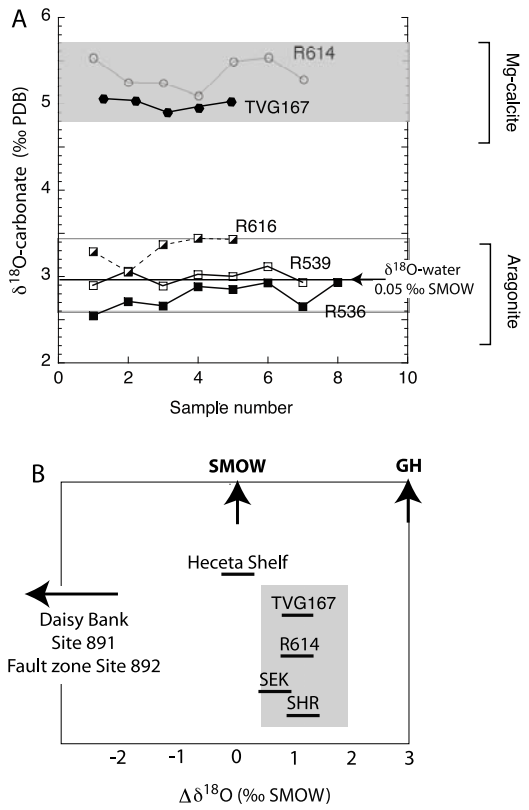

Figure 5. (a) Oxygen isotopic composition of aragonite (R536, R539, and R616) and Mg-calcite (R614) samples from Heceta Bank (region 1 in Figure 1) and for a Mg-calcite (TVG167) sample from the BSR outcrop site at 45°N (region 2 in Figure 1). The range of values obtained for aragonite samples reflect precipitation in equilibrium with seawater temperature of 7°C and $\delta^{18}O_{water}$ of 0.08 ± 0.5‰ SMOW, and the average isotopic value of 2.98‰ PDB reflects precipitation from $\delta^{18}O_{water}$ of 0.05‰ SMOW. (b) Deviations of the oxygen isotopic from equilibrium at present seawater conditions ($\Delta\delta^{18}O = \delta^{18}O_{estimated} - \delta^{18}O_{equilibrium}$). The Heceta shelf carbonates precipitate in equilibrium with bottom seawater, whereas the samples recovered in the upper slope are enriched in ^{18}O, revealing a significant contribution of water released by gas hydrate destabilization. Samples collected from topographic highs in the accretionary margin (SEK, South East Knoll; SHR, southern Hydrate Ridge; see Figure 1 for location) also bear the heavy $\delta^{18}O$ signal indicative of gas hydrate influence [*Bohrmann et al.*, 1998; *Greinert et al.*, 2002]. Carbonates recovered from Daisy bank and ODP Sites 891 and 892 are significantly lighter in $\delta^{18}O$ because of precipitation at higher than bottom water temperatures from fluids depleted in ^{18}O [*Sample and Kopf*, 1995]. SMOW indicates present seawater value of 0.08‰, and GH denotes hydrate cage water of 0.3‰ [*Davidson et al.*, 1983].

oxygen isotopic composition significantly heavier than that of the aragonite samples (Figure 5a). The oxygen isotopic composition of the water from which this phase precipitated can be estimated assuming a bottom water temperature of 4.5°C and using the equations of *Friedman and Oneil* [1977] corrected for the Mg content after *Tarutani et al.* [1969]. Such calculations indicate that the water from which the Mg-calcite precipitated is enriched relative to bottom water by 1.1 ± 0.4‰ SMOW.

[32] Clay dehydration reactions are known to release water that is isotopically enriched in ^{18}O. Such heavy pore fluids have been reported in deep sediments offshore Costa Rica ($\delta^{18}O$ = 5 to 7‰), and are recorded in carbonate deposits fed by these ascending fluids [*Han et al.*, 2004]. However, on the Cascadia margin, fluids recovered by drilling between 20 to 400 mbsf have an isotopic composition that ranges from 0 to −1‰ SMOW [*Tomaru et al.*, 2006], and furthermore the carbonates fed by ascending deep fluids are known to be highly depleted in ^{18}O. Thus the observed enrichment in the ^{18}O in sample R614 likely reflects fluids modified by gas hydrate destabilization, which yields cage water with an oxygen isotopic composition of +3.0‰ [*Davidson et al.*, 1983]. Indeed fluid samples recovered from ODP Leg 204, show discrete zones of water enriched in ^{18}O ($\delta^{18}O$ = 0 to +2.8‰), which coincide with pore water freshening signals indicative of significant gas hydrate dissociation [*Tomaru et al.*, 2006]. Enrichment in ^{18}O has also been previously observed in carbonates that occur in association with gas hydrate deposits in the Cascadia margin [*Bohrmann et al.*, 1998; *Greinert et al.*, 2002] and elsewhere [e.g., *Matsumoto*, 1989; *Aloisi et al.*, 2000; *Formolo et al.*, 2004].

[33] Gas hydrates are usually associated with a bottom-simulating reflector (BSR) in seismic data, which occurs where the geothermal gradient intercepts the thermodynamic gas hydrate stability boundary [e.g., *Hyndman and Spence*, 1992]. This reflector thus defines the lower limit of gas hydrate stability within the sediments. In the Oregon margin, the prevailing bottom water temperatures place the upper boundary for stability of methane hydrate at approximately 550 ± 60 m [*Tréhu et al.*, 1995]. The only available seismic data across Heceta Bank was acquired in 1975 and 1980, and the processed lines are available from the USGS (Figure 6). On lines WO34 and WO10, the BSR is seen only at water depths >1000 m. However, on

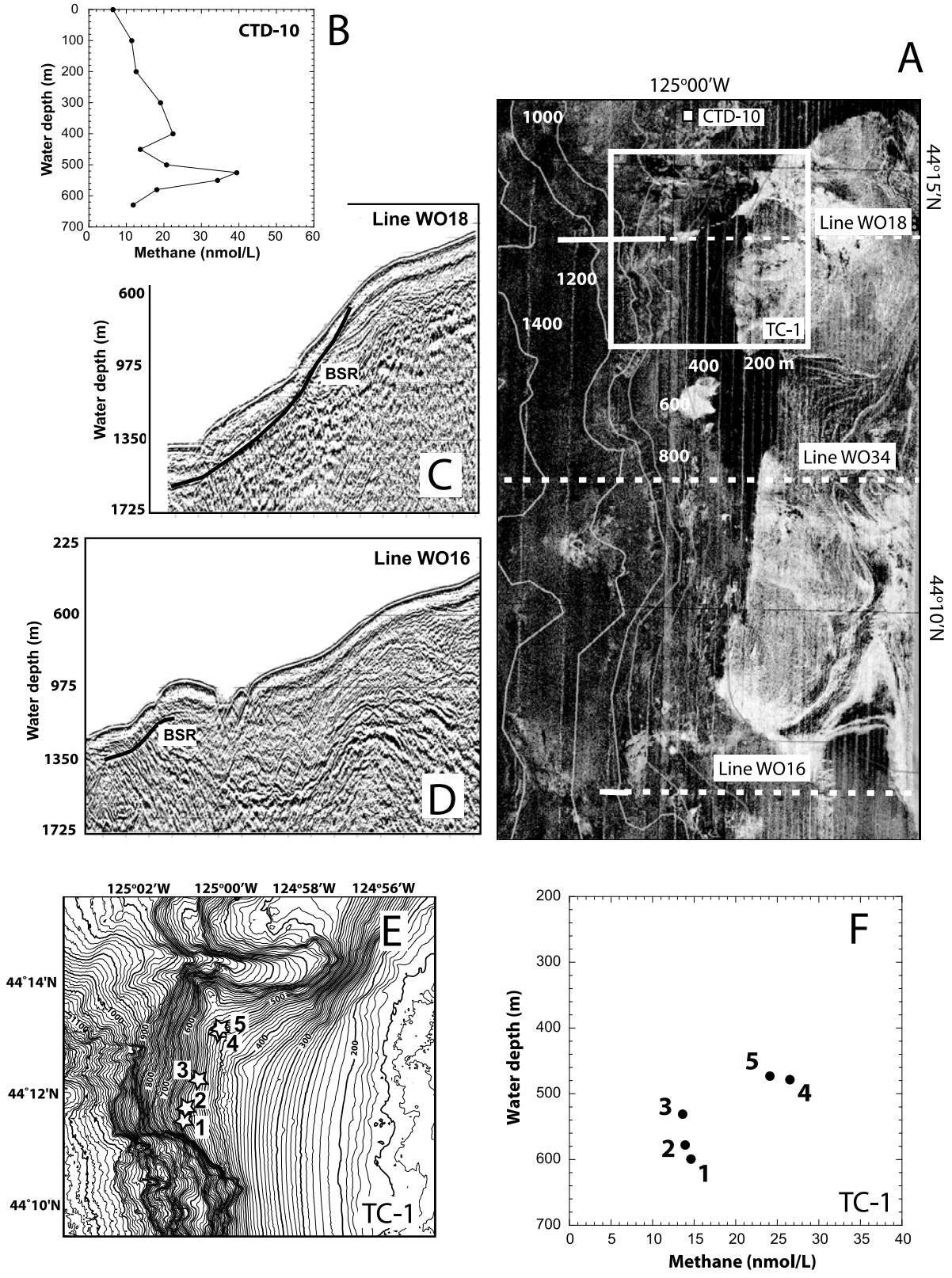
A
125°00'W
44°15'N
44°10'N
CTD-10
Line WO18
Line WO34
Line WO16
TC-1
1000
1200
1400
400
200 m
600
800
B
Water depth (m)
Methane (nmol/L)
C
BSR
D
E
125°02'W
125°00'W
124°58'W
124°56'W
44°14'N
44°12'N
44°10'N
F
Water depth (m)
Methane (nmol/L)

Figure 6

line WO18 a BSR is seen to shallow and approach the seafloor at ~600 m depth at a location of high backscatter indicative of carbonate deposition. A survey of this area using the WHOI TowCam revealed the presence of clam colonies and carbonate deposits associated with high-backscatter zones (Figure 6a). A hydrocast in this area show high methane levels between 500 and 600 m (Figure 6b), consistent with enhanced methane values measured in water samples collected near the seafloor during the TowCam survey (Figures 6e and 6f).

[34] We postulate that the occurrence of methane seeps along the upper slope region between 43°N and 45°N is triggered by the presence of a buried ridge moving with the subducting plate, as described by *Fleming and Tréhu* [1999] (Figure 7). Collision of the ridge with the Siletz Terrane, an oceanic plateau that was accreted to North America ~50 million years ago [*Snavely*, 1987], results in underplating and uplift of sediment sequences in the oncoming plate, which bear microbial methane. Associated with the tectonic uplift, there is a decrease in hydrostatic pressure at the seafloor, which leads to a marked reduction in methane solubility and in destabilization of gas hydrates. Along the upper slope microbial methane exolution may feed shallow vents. At depths shallower than 500 m, this methane gas vents at the seafloor in type II seeps, such as that surveyed during ROPOS Dive 536. Deeper than 550 ± 60 m, the methane is sequestered as gas hydrate, which may be subsequently destabilized by sediment uplift. The methane release would lead to seepage and carbonate formation along the 550 ± 60 m benthic corridor imaged as high-reflectivity zones (Figure 2a), in what we describe as type IV seeps.

4.6. Comparison With the Daisy Bank Region

[35] A series of water column surveys were conducted in the Daisy Bank region (region 2 in Figure 1), as part of a survey focused on methane venting from Hydrate Ridge [*Heeschen et al.*, 2005]. Their multiyear survey (7 cruises; 130 hydrocasts) revealed a complex system that includes a shallow methane source near the shelf, as well as the presence of a prevalent maximum between 400 and 600 m of water. The methane plume from the shelf and upper slope contains mixtures of local biogenic and thermogenic sources (δ^{13}C-CH_4 ranging from −56 to −28‰ PDB), with some isotopic modification due to aerobic methane oxidation in the water column.

[36] The observation of a BSR outcropping at the upper boundary for stability of methane hydrate was reported by *Tréhu et al.* [1995] on a multichannel seismic survey along 45°N (Figure 8). The location where the BSR outcrops at the seafloor at 45°N was surveyed using the German video sled OFOS (Ocean Floor Observation System) during cruise SO143 of the R/V *Sonne* [*Bohrmann et al.*, 2000]. The survey revealed abundant clam patches, bacterial mats and extensive carbonate formation. Similar to our observations in Heceta Bank, the distribution of carbonates in this region of the slope was in good agreement with inferences based on side-scan sonar data [*Bohrmann et al.*, 2000]. A TV-guided grab sampled carbonates from 567 mbsf (TVG-167-1, Table 1) at the BSR outcrop site and abundant vesicomyid specimens, characteristic of chemosynthetic communities [*Bohrmann et al.*, 2000]. Similar to Sample R614, the oxygen isotopic values of the Mg-calcite recovered by TVG-167 (δ^{18}O = 4.99 ± 0.06‰, Table 3) are heavier than predicted on the basis of formation in equilibrium with bottom seawater, consistent with a methane hydrate fingerprint. Two hydrocasts (stations NH30 and SO143-20 in Figure 8c) taken at this location by *Heeschen et al.* [2005], show evidence of methane discharge at mid water depth, which may reflect input at the BSR outcrop site, which supports chemosynthetic communities. Water samples were also collected within 4 m of the seafloor with the WHOI TowCam, from two additional zones characterized by high-backscatter signals in this region of the margin (Figure 8a). The samples show enhanced methane levels between 450 and 600 m, supporting a localized discharge of methane, that may be the source for the midwater methane maxima observed in the water column

Figure 6. (a) Backscatter intensity of Heceta Bank, increasing from dark to lighter shades, showing locations of seismic lines WO18, WO34, and WO16; hydrocast station (CTD-10); and TowCam survey region (box with white borders). (b) Methane concentration at hydrocast station CTD-10. (c) Seismic line WO18 showing a BSR that approaches the seafloor at ~600 m water depth at a location that corresponds to high-reflectivity data. (d) In lines WO16 and WO34 (not shown) the BSR is at >1000 m of water depth. (e) Station locations along a TowCam survey TC-1, covering the 500 to 600 m region of high backscatter where the BSR outcrops at the seafloor on line WO18. (f) Methane data from water samples collected within 4 m of the seafloor during the TowCam survey in the region shown in Figure 6e.

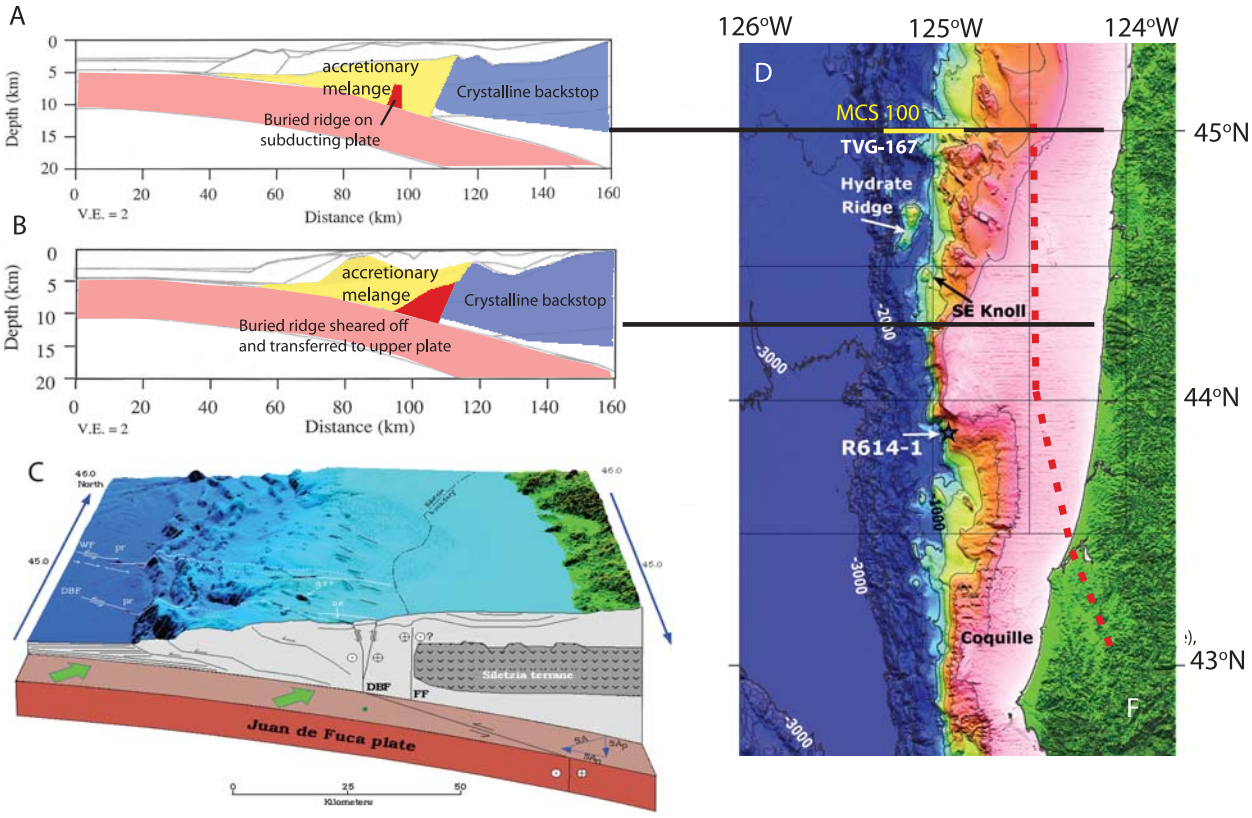

Figure 7. (a and b) Tectonic model of *Fleming and Tréhu* [1999], based on magnetic and gravity data. A buried ridge (red) is transported with the subducting plate (pink), uplifting the overlying accretionary complex. The yellow area demarks sediments with density >2.54 g/cm^3. When the ridge encounters the crystalline backstop of the Siletz Terrane (blue), it is sheared off and becomes part of the upper plate, inhibiting sediment subduction. (c) Cross section illustrating subduction of the Juan de Fuca plate and location of the Siletz Terrain. Carbonates recovered along the Daisy Bank Fault (DBF) are enriched in ^{13}C and depleted in ^{18}O, consistent with fluid migration along these deep seated faults. FF denotes location of the Fulmar fault. (d) Bathymetric map delineating the extent of the region where a N–S trending basaltic ridge is thought to be buried beneath the accretionary complex. It denotes the location of MCS line 100 (yellow), seaward edge of the Siletz Terrane (broken red line), and seepage sites where carbonate samples (R614 and TVG167) with a gas hydrate fingerprint were recovered. Sediment uplift associated with the buried ridge is thought to result in methane exolution, transport, and gas hydrate formation.

data (Figure 8c). This data set provides additional evidence for methane seepage, which may be linked to destabilization of gas hydrate in the upper slope from 43°N to 45°N.

4.7. Role of Tectonics on Methane Release

[37] It has long been known that earthquake activity, faulting, and uplift impact fluid flow, gas solubility and gas hydrate dynamics, and thus play a major role on modulating the release of hydrocarbons at seafloor vents. Fluid migration associated with faults and other high-permeability zones plays a clear role in the transport of methane and other hydrocarbons to the hydrate stability zone and to the seafloor [e.g., *Riedel et al.*, 2002; *Xie et al.*, 2003; *von Rad et al.*, 2000]. Earthquake activity and associated slumping may lead to gas hydrate destabilization in active margins, with subsequent release of gas [*Johnson*, 2004]. Tectonic uplift can also play a significant role in sediment stability and gas hydrate dynamics, as both gas hydrate stability and methane solubility are highly impacted by pressure changes. For example, sediment uplift during accretion of the Makran prism is thought to have destabilized gas hydrate at the base of stability field, leading to the observed accumulations of free gas beneath the BSR [*Sain et al.*, 2000]. Similarly, the observation of a BSR on regions of tectonic uplift in the Peru margin has been attributed to gas release in these areas, as no

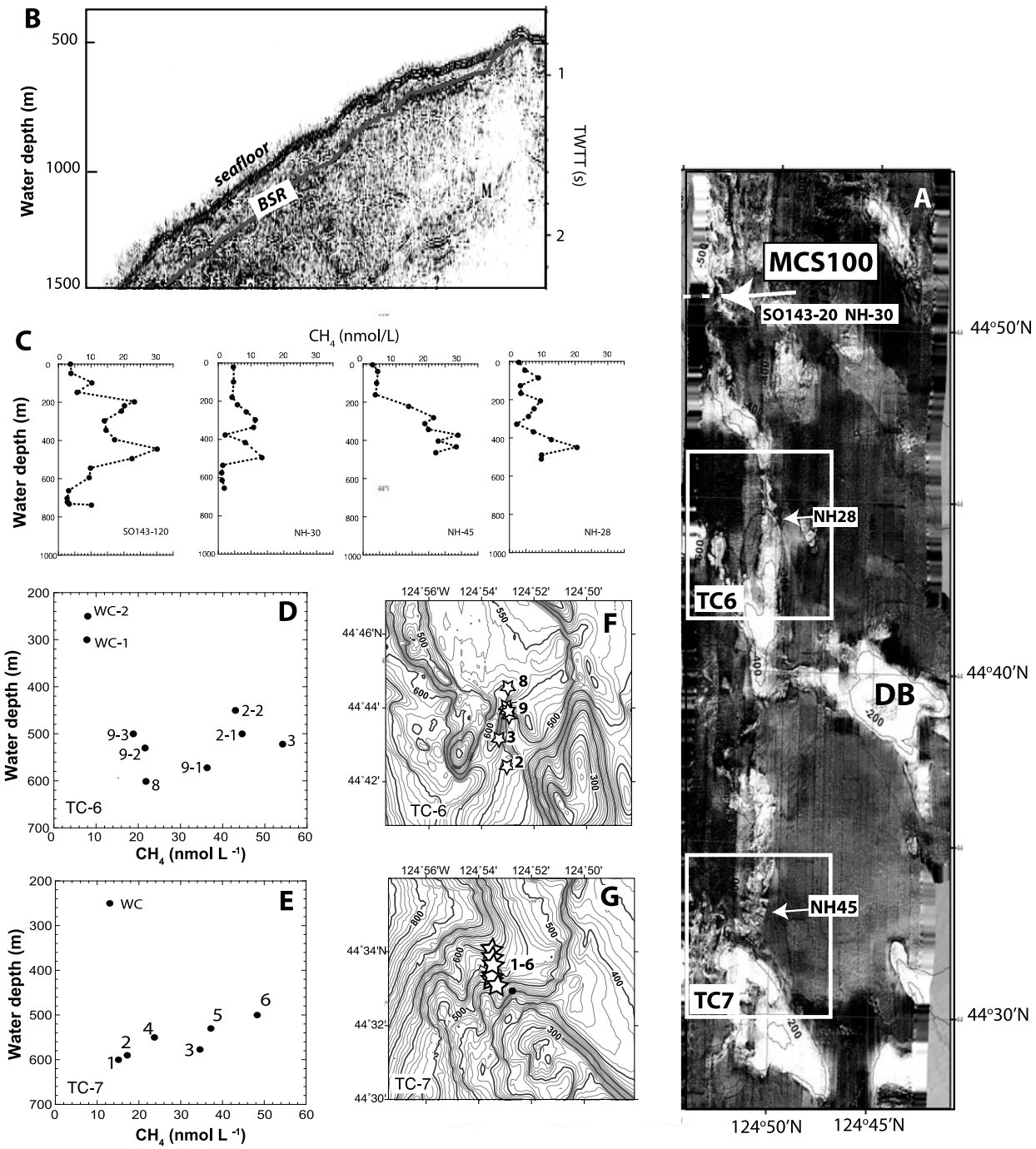

Figure 8. (a) Backscatter intensity of region 2, increasing from dark to lighter shades (data from *Lanier et al.* [2007]), showing location of seismic line 100; Daisy Bank (DB); TowCam surveys TC6 and TC7; and hydrocast stations SO143-120, NH30, NH28, and NH45. (b) Seismic section (MCS line 100) across the midslope region at 44°51′N, where a strong BSR is observed as it shoals and breaches the seafloor at ∼500 m [from *Tréhu et al.*, 1995]. (c) Methane profiles from hydrocasts [from *Heeschen et al.*, 2005]. (d and e) Methane concentrations from the water column (WC) and within 4 m of the seafloor during TowCam surveys TC6 and TC7. (f and g) Bathymetry and station designation for methane data of Figures 8d and 8e.

BSR is apparent in seismic records from neighboring rapidly subsiding basins [*von Huene and Pecher*, 1999]. Offshore Chile, tectonic uplift and associated changes in the gas hydrate stability zone result in a BSR that is discontinuous and in some areas appears as a double reflector [*Rodrigo et al.*, 2009]. Models based on proposed transient uplift of the north Atlantic during the latest Paleocene have been developed to demonstrate that large quantities of carbon (>2000 Gt) could have been released from gas hydrate reservoirs and could account for the magnitude and timing of the carbon isotopic excursion associated with the Paleocene-Eocene Thermal Maximum [*Maclennan and Jones*, 2006].

[38] In the scenario we propose for the Heceta Bank region, tectonic uplift drives methane exolution at the critical upper limit of gas hydrate stability, which facilitates the slope failure in response to ridge subduction. The EM300 survey (Figures 2 and 4) reveals a series of slide scars on the SW region of the bank, which are interpreted to represent continued mass wasting of a megaslide headwall described by *Goldfinger et al.* [2000]. The excess pore pressure that is generated by gas exolution at the upper limit of gas hydrate stability may act as a triggering mechanism for slope failure, and may be in part responsible for the Heceta megaslide, which exposes scar fronts along the 550 ± 60 m corridor. This scenario is in some aspects similar to the mechanisms proposed for the gravitational displacement of large volumes of sediment on the eastern Nankai slope by *Cochonat et al.* [2002]. Here, subduction of a paleo-Zenisu ridge, led to rapid uplift of the seafloor at the origin of the steep slope observed [*Mazzotti et al.*, 1999]; changes in the mechanical behavior of the sediment due to gas hydrate destabilization in response to pressure changes is thought to decrease shear strength at the depth corresponding to the BSR enough to induce slope failure [*Cochonat et al.*, 2002]. Subduction of seamounts and ridges is also reported in the gas hydrate bearing regions offshore Costa Rica [*Dominguez et al.*, 1998] and the Hikurangi margin [*Barnes et al.*, 2009]; the resulting uplift associated with this process is likely to have a major effect on gas hydrate stability, gas accumulation and slope failures in these regions and elsewhere.

4.8. Comparison With Other Areas Along the Northeast Pacific Margin

[39] Seeps along the Oregon-Washington continental margin encompass systems fed by two distinct methane sources, which vent in response to different forcing mechanisms. Namely, venting of thermogenic gases probably generated from Eocene and/or Oligo-Miocene mélanges underlying most shelf regions, and methane generated from younger sequences in the modern accretionary margin and which support gas hydrate-related seeps along the slope.

[40] Available carbon isotopic data collected from gas seeps and carbonates along the convergent eastern Pacific margin also indicate the presence of these two contrasting methane sources (Figure 1). Drilling of exploratory wells in the Tofino Basin off Vancouver Island recovered samples that contain kerogen with a low hydrogen index, which clearly identified the source rocks as the underlying Miocene and Oligocene strata [*Bustin*, 1995]. Analyses of vent gas and gas hydrate deposits recovered at a seep on the Barkley canyon document fluid migration from a deep petroleum reservoir in the Tofino Basin to the seafloor of Barkley canyon [*Pohlman et al.*, 2005]. This thermogenic gas hydrate deposit contrasts with the gas hydrate recovered at the Bullseye vent in the slope region of the margin, where isotopic composition of vent gases, gas hydrate and associated carbonates reveal a biogenic source for the methane at this site [*Riedel et al.*, 2006].

[41] At the southern end of the Cascadia accretionary prism, the Eel River Basin is underlain by rocks of the Franciscan complex, late Jurassic to Eocene in age, which, in turn, is overlain by about 4000 m of Neogene marine mudstone, siltstone and fine sandstone [*McCulloch*, 1987]. Thermogenic hydrocarbon seeps here were first described in a diapiric structure on the Eel Plateau at ~650 m of water by *Kvenvolden and Field* [1981]; *Collier and Lilley* [2005] report seepage of isotopically heavy methane at Table Bluff seep (43 m deep), near the Eel River mouth. In contrast with these thermogenic seeps, *Brooks et al.* [1991] document the presence of gas hydrates in piston cores collected at 510 to 542 m of water with an isotopic composition that reflects a biogenic source. Carbonate samples recovered from this area span a large range of isotopic compositions [e.g., *Orphan et al.*, 2004; *Gieskes et al.*, 2005], consistent with the heterogeneity of methane sources in this basin.

5. Conclusions

[42] Newly acquired bathymetric and ROPOS surveys on the Heceta Bank offshore Oregon are

interpreted in the context of a rich data set available for the margin on structural features, sediment accretion, methane and seep carbonates and gas hydrates. Two main conclusions arise from this composite analysis:

[43] 1. The northeast Pacific margin from Vancouver to California receives significant input of methane from two distinct sources, which can be identified by the isotopic composition of the carbon in carbonate deposits and the methane that leads to their formation and seeps at the seafloor. An eastward source, characterized by a thermogenic methane component, is juxtaposed to methane generated by microbial decomposition of organic carbon in sediments of the accreted prism. These two methane supply systems, previously recognized in water column surveys [*Heeschen et al.*, 2005] play a significant role in the carbon cycling and methane inventories of the margin and are likely to respond to different forcing mechanisms.

[44] 2. The location of methane seeps at the upper limit of gas hydrate stability and associated carbonates bear the mark of gas hydrate dissociation. We propose a scenario whereby the collision of a buried ridge with the Siletz Terrane [*Fleming and Tréhu*, 1999] results in uplift of gas hydrate bearing sediment sequences on the oncoming plate. The pressure decrease leads to gas hydrate dissociation, with concomitant methane release at the upper limit of gas hydrate stability. Oxidation of this methane source results in the formation of carbonates, which are probably the cause of the high backscatter observed along the 550 ± 60 m contour offshore Heceta Bank. The excess pore pressured caused by gas hydrate dissociation in this region of the slope may facilitate slope failure in response to earthquakes and seamount collision.

Acknowledgments

[45] The EM300 survey of Heceta Bank was funded by the Northwest Fisheries Science Center (National Marine Fisheries Service) and the Oregon SeaGrant Program. Funding for the ROPOS dives was provided by the West Coast and Polar Undersea Research Center of NOAA's National Undersea Research Program. Two of the authors (R.E. and S.M.) were supported for this project by the NOAA VENTS Program and NOAA's Office of Ocean Exploration. Additional funding was received from NSF grants OCE-0550402, OCE-0646226, and OCE-0628700 and the National Energy and Technology Laboratory of the DOE. We thank C&C Technology, the Canadian Scientific Support Facility, and the personnel and science teams of the R/V *Ocean Alert* and NOAA ship *Ronald H. Brown* for their excellent support in at-sea data acquisition and initial processing. Dave Clague and Norman Maher (MBARI) provided logistical and computer support, as well as providing additional time on site, which greatly enhanced the success of the program. We gratefully acknowledge the support of John Hughes Clark and Larry Mayer on EM-300 data processing and of Anne Valdez and Shana Goffredi on bivalve identification. The manuscript benefited from insightful comments from W. Wakefield (who also served as co–chief scientist on the 2000–2001 expeditions), J. Sample, and an anonymous reviewer. This paper is PMEL contribution 3440.

References

Aloisi, G., J. P. Foucher, J. Woodside, C. Pierre, and J. M. Rouchy (2000), Methane-related authigenic carbonates of eastern Mediterranean Sea mud volcanoes and their possible relation to gas hydrate destabilization, *Earth Planet. Sci. Lett.*, *184*, 321–338, doi:10.1016/S0012-821X(00)00322-8.

Barnes, P. M., G. Lamarche, J. Bialas, S. Henrys, I. Pecher, G. L. Netzeband, J. Greinert, J. Mountjoy, K. Pedley, and G. Crutchley (2009), Tectonic and geological framework for gas hydrates and cold seeps on the Hikurangi Subduction Margin, New Zealand, *Mar. Geol.*, doi:10.1016/j.margeo.2009.03.012, in press.

Beget, J. E., and J. A. Addison (2007), Methane gas release from the Storegga submarine landslide linked to early Holocene climate change: A speculative hypothesis, *Holocene*, *17*(3), 291–295.

Boetius, A., and E. Suess (2004), Hydrate Ridge: A natural laboratory for the study of microbial life fueled by methane from near-surface gas hydrates, in *Geomicrobiology and Biogeochemistry of Gas Hydrates and Hydrocarbon Seeps*, edited by C. Zhang and B. Lanoil, *Chem. Geol.*, *205*, 91–310.

Boetius, A., K. Ravenschlag, C. J. Schubert, D. Rickert, F. Widdel, A. Gieseke, R. Amann, B. B. Jørgensen, U. Witte, and O. Pfannkuche (2000), A marine consortium apparently mediating anaerobic oxidation of methane, *Nature*, *407*, 623–626, doi:10.1038/35036572.

Böhm, F., A. Eisenhauer, H. Lehnert, J. Reitner, G. Wörheide, M. M. Joachimski, and W. C. Dullo (2000), Oxygen isotope fractionation in marine aragonite of coralline sponges, *Geochim. Cosmochim. Acta*, *64*, 1695–1703, doi:10.1016/S0016-7037(99)00408-1.

Bohrmann, G., J. Greinert, E. Suess, and M. E. Torres (1998), Authigenic carbonates from the Cascadia subduction zone and their relation to gas hydrate stability, *Geology*, *26*, 647–650, doi:10.1130/0091-7613(1998)026<0647:ACFTCS>2.3.CO;2.

Bohrmann, G., P. Linke, E. Suess, and O. Pfannkuche (2000), RV Sonne cruise report SO143 ''TECFLUX-I-1999'', *Rep. 93*, Leibniz Inst. of Mar. Sci. at Univ. of Kiel (IFM-GEOMAR), Kiel, Germany.

Brooks, J. M., M. E. Field, and M. C. Kennicutt, II (1991), Observations of gas hydrates in marine sediments, offshore north California, *Mar. Geol.*, *96*, 103–109, doi:10.1016/0025-3227(91)90204-H.

Bustin, R. M. (1995), Organic maturation and petroleum source rock potential of Tofino Basin, southwestern British Columbia, *Bull. Can. Pet. Geol.*, *43*, 177–186.

Campbell, K. A. (2006), Hydrocarbon seep and hydrothermal vent paleoceano-environments: Past developments and future research directions, *Palaeogeogr. Palaeoclimatol. Palaeoecol.*, *232*, 362–407, doi:10.1016/j.palaeo.2005.06.018.

Campbell, K. A., J. D. Farmer, and D. Des Marais (2002), Ancient hydrocarbon seeps from the Mesozoic convergent margin of California: Carbonate geochemistry, fluids and paleoenvironments, *Geofluids*, *2*, 63–94, doi:10.1046/j.1468-8123.2002.00022.x.

Chevallier, J., A. M. Tréhu, N. L. Bangs, J. E. Johnson, and H. J. Meyer (2006), Seismic sequence stratigraphy and tectonic evolution of southern Hydrate Ridge [online], *Proc. Ocean Drill. Program Sci. Results, 204*, 29 pp., doi:10.2973/odp.proc.sr.204.121.2006. (Available at http://www-odp.tamu.edu/publications/204_SR/121/121.htm)

Claypool, G. E., and I. R. Kaplan (1974), The origin and distribution of methane in marine sediments, in *Natural Gases in Marine Sediments*, edited by I. R. Kaplan, pp. 99–139, Plenum, New York.

Claypool, G. E., A. V. Milkov, Y.-J. Lee, M. E. Torres, W. S. Borowski, and H. Tomaru (2006), Microbial methane generation and gas transport in shallow sediments of an accretionary complex, Southern Hydrate Ridge (ODP Leg 204), offshore Oregon, USA [online], *Proc. Ocean Drill. Program Sci. Results, 204*, 52 pp. (Available at http://www-odp.tamu.edu/publications/204_SR/113/113.htm)

Cochonat, P., H. Nouze, C. Fouchet, J. P. Foucher, J.-P. Cadet, S. J. Lallemant, and S. Mazzotti (2002), Slope instabilities and gravity processes in fluid migration and tectonically active environment in the eastern Nankai accretionary wedge (KAIKO-Tokai'96 cruise), *Mar. Geol.*, *187*(1–2), 193–202.

Collier, R. W., and M. D. Lilley (2005), Composition of shelf methane seeps on the Cascadia Continental Margin, *Geophys. Res. Lett.*, *32*, L06609, doi:10.1029/2004GL022050.

Colwell, F. S., M. E. Delwiche, D. W. Reed, D. T. Newby, and T. J. Phelps (2008), Estimates of biogenic methane production rates in deep marine sediments at Hydrate Ridge, Cascadia margin, *Appl. Environ. Microbiol.*, *74*, 3444–3452, doi:10.1128/AEM.02114-07.

Dählmann, A., and G. J. de Lange (2003), Fluid-sediment interactions at eastern Mediterranean mud volcanoes: A stable isotope study from ODP Leg 160, *Earth Planet. Sci. Lett.*, *212*, 377–391, doi:10.1016/S0012-821X(03)00227-9.

Davidson, D. W., D. J. Leaist, and R. Hesse (1983), Oxygen-18 enrichment in water of a clathrate hydrate, *Geochim. Cosmochim. Acta*, *47*, 2293–2295, doi:10.1016/0016-7037(83)90053-4.

Dickens, G. R., and M. S. Quinby-Hunt (1994), Methane hydrate stability in seawater, *Geophys. Res. Lett.*, *21*, 2115–2118, doi:10.1029/94GL01858.

Dillon, W., and C. Paull (1983), Marine gas hydrates II: Geophysical evidence, in *Natural Gas Hydrates—Properties, Occurrences and Recovery*, edited by J. Cox, pp. 73–90, Butterworth, Boston, Mass.

Dominguez, S., S. E. Lallemand, J. Malavieille, and R. von Huene (1998), Upper plate deformation associated with seamount subduction, *Tectonophysics*, *293*, 207–224, doi:10.1016/S0040-1951(98)00086-9.

Etiope, G., and A. V. Milkov (2004), A new estimate of global methane flux from onshore and shallow submarine mud volcanoes to the atmosphere, *Environ. Geol.*, *46*(8), 997–1002.

Fleming, S. W., and A. M. Tréhu (1999), Crustal structure beneath the central Oregon convergent margin from potential-field modeling: Evidence for a buried basement ridge in local contact with a seaward dipping backstop, *J. Geophys. Res.*, *104*, 20,431–20,447, doi:10.1029/1999JB900159.

Formolo, M. J., C. Kelley, R. Sassen, J. Horita, D. R. Cole, T. W. Lyons, and C. Zhang (2004), Quantifying carbon sources in the formation of authigenic carbonates at gas hydrate sites in the Gulf of Mexico, *Chem. Geol.*, *205*, 253–264, doi:10.1016/j.chemgeo.2003.12.021.

Friedman, I., and J. R. Oneil (1977), Compilation of stable isotope fractionation factors of geochemical interest, *U.S. Geol. Surv. Prof. Pap., 440-kk*.

Gieskes, J., J. B. Martin, J. Greinert, A. Rathburn, B. McAdoo, C. Mahn, and S. Day (2005), A study of the chemistry of pore fluids and authigenic carbonates in methane seep environments: Kodiak Trench, Hydrate Ridge, Monterey Bay, and Eel River Basin, *Chem. Geol.*, *220*, 329–345, doi:10.1016/j.chemgeo.2005.04.002.

Goldfinger, C., M. E. MacKay, G. F. Moore, L. D. Kulm, S. S. Yeats, and B. Appelgate (1992), Transverse structural trends along the Oregon convergent margin: Implications for Cascadia earthquake potential and crustal rotations, *Geology*, *20*, 141–144, doi:10.1130/0091-7613(1992)020<0141:TSTATO>2.3.CO;2.

Goldfinger, C., C. Hummon, L. D. Kulm, R. S. Yeats, and L. McNeill (1997), Oblique strike-slip faulting of the central Cascadia submarine forearc, *J. Geophys. Res.*, *102*, 8217–8243, doi:10.1029/96JB02655.

Goldfinger, C., L. D. Kulm, L. C. McNeill, and P. Watts (2000), Super-scale failure of the southern Oregon Cascadia margin, *Pure Appl. Geophys.*, *157*, 1189–1226, doi:10.1007/s000240050023.

Greinert, J., G. Bohrmann, and M. Elvert (2002), Stromatolitic fabric of authigenic carbonate crusts: Result of anaerobic methane oxidation at cold seeps in 4,850 m water depth, *Int. J. Earth Sci.*, *91*, 698–711, doi:10.1007/s00531-001-0244-9.

Han, X., E. Suess, H. Sahling, and K. Wallmann (2004), Fluid venting activity on the Costa Rica margin: New results from authigenic carbonates, *Int. J. Earth Sci.*, *93*, 596–611.

Heeschen, K. U., R. W. Collier, M. A. DeAngelis, E. Suess, G. Rehder, P. Linke, and G. P. Klinkhammer (2005), Methane sources, distributions, and fluxes from cold vent sites at Hydrate Ridge, Cascadia Margin, *Global Biogeochem. Cycles*, *19*, GB2016, doi:10.1029/2004GB002266.

Hinrichs, K.-U., J. M. Hayes, S. P. Sylva, P. G. Brewert, and E. F. DeLong (1999), Methane-consuming archaebacteria in marine sediments, *Nature*, *398*, 802–805, doi:10.1038/19751.

Hornafius, J. S., D. Quigley, and B. P. Luyendyk (1999), The world's most spectacular marine hydrocarbon seeps (Coal Oil Point, Santa Barbara Channel, California): Quantification of emissions, *J. Geophys. Res.*, *104*, 20,703–20,711, doi:10.1029/1999JC900148.

Hudson, J. C., and T. F. Anderson (1989), Ocean temperatures and isotopic composition through time, in *Environments and Physiology of Fossil Organisms*, edited by E. N. K. Clarkson, G. B. Curry, and W. D. I. Rolfe, *Trans. R. Soc. Edinburgh Earth Sci.*, *8*, 183–192.

Hughes-Clarke, J. E., L. A. Mayer, and D. E. Wells (1996), Shallow-water imaging multibeam sonars: A new tool for investigating seafloor processes in the coastal zone and on the continental shelf, *Mar. Geophys. Res.*, *18*, 607–629, doi:10.1007/BF00313877.

Hyndman, R. D., and G. D. Spence (1992), A seismic study of methane hydrate marine bottom simulating reflectors, *J. Geophys. Res.*, *97*, 6683–6698, doi:10.1029/92JB00234.

Johnson, J. E. (2004), Deformation, fluid venting and slope failure at an active margin gas hydrate province Hydrate Ridge Cascadia accretionary wedge, doctoral dissertation, 145 pp., Oreg. State Univ., Corvallis.

Johnson, J. E., C. Goldfinger, and E. Suess (2003), Geophysical constraints on the surface distribution of authigenic

carbonates across the Hydrate Ridge region, Cascadia margin, *Mar. Geol.*, *202*, 79–120, doi:10.1016/S0025-3227(03)00268-8.

Johnson, J. E., C. Goldfinger, A. M. Tréhu, N. L. B. Bangs, M. E. Torres, and J. Chevallier (2006), North-south variability in the history of deformation and fluid venting across Hydrate Ridge, Cascadia Margin [online], *Proc. Ocean Drill. Program Sci. Results, 204*, 16 pp. (Available at http://www-odp.tamu.edu/publications/204_SR/125/125.htm)

Jørgensen, B. B., and A. Boetius (2007), Feast and famine—Microbial life in the deep-sea bed, *Nat. Rev. Microbiol.*, *5*, 770–781, doi:10.1038/nrmicro1745.

Kennett, J. P., K. G. Cannariato, I. L. Hendy, and R. J. Behl (2003), *Methane Hydrates in Quaternary Climate Change: The Clathrate Gun Hypothesis*, 216 pp., AGU, Washington, D. C.

Kulm, L. D., and G. A. Fowler (1974), Oregon continental margin structure and stratigraphy: A test of the imbricate thrust model, in *The Geology of Continental Margins*, edited by C. A. Burk and C. L. Drake, pp. 261–283, Springer, New York.

Kulm, L. D., and E. Suess (1990), Relationship between carbonate deposits and fluid venting: Oregon accretionary prism, *J. Geophys. Res.*, *95*, 8899–8915, doi:10.1029/JB095iB06p08899.

Kulm, L. D., et al. (1986), Oregon subduction zone: Venting, fauna, and carbonates, *Science*, *231*, 561–566, doi:10.1126/science.231.4738.561.

Kvenvolden, K. A., and M. E. Field (1981), Thermogenic hydrocarbons in unconsolidated sediment of Eel river basin, offshore northern California, *Am. Assoc. Pet. Geol. Bull.*, *65*, 1642–1646.

Kvenvolden, K. A., and T. D. Lorenson (2001), The global occurrence of natural gas hydrate, in *Natural Gas Hydrates Occurrence, Distribution, and Detection*, *Geophys. Monogr. Ser.*, vol. 124, edited by C. K. Paull and W. P. Dillon, pp. 3–18, AGU, Washington, D. C.

Lanier, A., C. Romsos, and C. Goldfinger (2007), Seafloor habitat mapping on the Oregon continental margin: A spatially nested GIS approach to mapping scale, mapping methods, and accuracy quantification, *Mar. Geod.*, *30*, 51–76, doi:10.1080/01490410701296143.

Luff, R., K. Wallmann, and G. Aloisi (2004), Numerical modeling of carbonate crust formation at cold vent sites: Significance for fluid and methane budgets and chemosynthetic biological communities, *Earth Planet. Sci. Lett.*, *221*, 337–353, doi:10.1016/S0012-821X(04)00107-4.

MacKay, M. E. (1995), Structural variation and landward vergence at the toe of the Oregon accretionary prism, *Tectonics*, *14*, 1309–1320, doi:10.1029/95TC02320.

MacKay, M. E., G. F. Moore, G. R. Cochrane, J. C. Moore, and L. D. Kulm (1992), Landward vergence and oblique structural trends in the Oregon accretionary prism: Implications and effect on fluid flow, *Earth Planet. Sci. Lett.*, *109*, 477–491, doi:10.1016/0012-821X(92)90108-8.

Maclennan, J., and S. M. Jones (2006), Regional uplift, gas hydrate dissociation and the origins of the Paleocene-Eocene Thermal Maximum, *Earth Planet. Sci. Lett.*, *245*(1–2), 65–80.

Maslin, M., M. Owen, S. Day, and D. Long (2004), Linking continental-slope failures and climate change: Testing the clathrate gun hypothesis, *Geology*, *32*(1), 53–56.

Matsumoto, R. (1989), Isotopically heavy oxygen-containing siderite derived from the decomposition of methane hydrate, *Geology*, *17*, 707–710, doi:10.1130/0091-7613(1989)017<0707:IHOCSD>2.3.CO;2.

Mazzotti, S., P. Henry, X. Le Pichon, and T. Sagiya (1999), Strain partitioning in the zone of transition from Nankai subduction to Izu-Bonin collision (Central Japan): Implications for an extensional tear within the subducting slab, *Earth Planet. Sci. Lett.*, *172*, 1–10.

McCulloch, D. S. (1987), Regional geology and hydrocarbon potential of offshore central California, in *Geologic and Resource Potential of the Continental Margin of Western North America and Adjacent Ocean Basins—Beaufort Sea to Baja California*, edited by D. W. Scholl, A. Grantz, and J. G. Vedder, pp. 353–401, Circum-Pac. Counc. for Energy and Miner. Resour., Houston, Tex.

McNeill, L. C., C. Goldfinger, L. V. D. Kulm, and R. S. Yeats (2000), Tectonics of the Neogene Cascadia forearc basin: Investigations of a deformed late Miocene unconformity, *Geol. Soc. Am. Bull.*, *112*(8), 1209–1224.

Mienert, J., S. Bunz, S. Guidard, M. Vanneste, and C. Berndt (2005), Ocean bottom seismometer investigations in the Ormen Lange area offshore mid-Norway provide evidence for shallow gas layers in subsurface sediments, *Mar. Pet. Geol.*, *22*(1–2), 287–297.

Milkov, A. V., R. Sassen, T. V. Apanasovich, and F. G. Dadashev (2003), Global gas flux from mud volcanoes: A significant source of fossil methane in the atmosphere and the ocean, *Geophys. Res. Lett.*, *30*(2), 1037, doi:10.1029/2002GL016358.

Muehlberg, G. E. (1971), Structure and stratigraphy of Quaternary strata of the Heceta Bank, central Oregon shelf, Msc. thesis, 78 pp., Oreg. State Univ., Corvallis.

Orphan, V. J., C. H. House, K.-U. Hinrichs, C. K. Paull, W. Ussler III, and T. H. Naehr (2004), Geological, geochemical, and microbiological heterogeneity of the seafloor around methane vents in the Eel River Basin, offshore California, *Chem. Geol.*, *205*, 265–289, doi:10.1016/j.chemgeo.2003.12.035.

Pearcy, W. G., D. L. Stein, M. A. Hixon, E. K. Pikitch, W. H. Barss, and R. M. Starr (1989), Submersible observations of deep-reef fishes of Heceta Bank, Oregon, *Fish. Bull.*, *87*, 955–965.

Pecher, I. A., C. R. Ranero, R. von Huene, T. A. Minshull, and S. C. Singh (1998), The nature and distribution of bottom simulating reflectors at the Costa Rican convergent margin, *Geophys. J. Int.*, *133*(2), 219–229.

Pecher, I. A., K. Faure, G. J. Massoth, J. Greinert, S. M. Ellis, S. A. Henrys, S. M. Chiswell, and N. Kukowski (2005), Seafloor erosion at the top of gas hydrate stability and its implications, Rock Garden and Ritchie Banks, Hikurangi margin, paper presented at Symposium of the New Zealand Geophysical Society, Lower Hutt, New Zealand, 27 and 28 Oct.

Pohlman, J. W., E. A. Canuel, N. R. Chapman, G. D. Spence, M. J. Whiticar, and R. Coffin (2005), The origin of thermogenic gas hydrates on the northern Cascadia margin as inferred from isotopic ($^{13}C/^{12}C$ and D/H) and molecular composition of hydrate and gas vent, *Org. Geochem.*, *36*, 703–716, doi:10.1016/j.orggeochem.2005.01.011.

Popp, B. N., F. J. Sansone, T. M. Rust, and D. A. Merritt (1995), Rapid method for determining abundance and carbon isotopic composition of dissolved methane in sediments and nearshore waters, *Anal. Chem.*, *67*, 405–411, doi:10.1021/ac00098a028.

Rao, Y. H., C. Subrahmanyam, A. Rastogi, and B. Deka (2002), Slope failures along the western continental margin of India: A consequence of gas-hydrate dissociation, rapid sedimentation rate, and seismic activity?, *Geo Mar. Lett.*, *22*(3), 162–169.

Riedel, M., G. D. Spence, N. R. Chapman, and R. D. Hyndman (2002), Seismic investigations of a vent field associated with gas hydrates, offshore Vancouver Island, *J. Geophys. Res.*, *107*(B9), 2200, doi:10.1029/2001JB000269.

Riedel, M., R. D. Hyndman, I. Novosel, G. D. Spence, R. N. Chapman, R. C. Solem, and T. Lewis (2006), Geophysical and geochemical signatures associated with gas hydrate-related venting in the northern Cascadia margin, *Bull. Geol. Soc. Am.*, *118*, 23–38, doi:10.1130/B25720.1.

Rodrigo, C., A. Gonzalez-Fernandez, and E. Vera (2009), Variability of the bottom-simulating reflector (BSR) and its association with tectonic structures in the Chilean margin between Arauco Gulf (37°S) and Valdivia (40°S), *Mar. Geophys. Res.*, *30*(1), 1–19.

Sain, K., T. A. Minshull, S. C. Singh, and R. W. Hobbs (2000), Evidence for a thick free gas layer beneath the bottom simulating reflector in the Makran accretionary prism, *Mar. Geol.*, *164*(1–2), 3–12.

Sample, J. C., and A. Kopf (1995), Isotope geochemistry of syntectonic carbonate cements and veins from the Oregon Margin: Implications for the hydrogeologic evolution of the accretionary wedge, *Proc. Ocean Drill. Program Sci. Results*, *146*, 137–148.

Sample, J. C., and M. R. Reid (1998), Contrasting hydrogeologic regimes along strike-slip and thrust faults in the Oregon convergent margin: Evidence from the chemistry of syntectonic carbonate cements and veins, *Geol. Soc. Am. Bull.*, *110*, 48–59, doi:10.1130/0016-7606(1998)110<0048:CHRASS>2.3.CO;2.

Sample, J. C., M. R. Reid, H. J. Tobin, and J. C. Moore (1993), Carbonate cements indicate channeled fluid flow along a zone of vertical faults at the deformation front of the Cascadia accretionary wedge (northwest U.S. coast), *Geology*, *21*, 507–510, doi:10.1130/0091-7613(1993)021<0507:CCICFF>2.3.CO;2.

Sassen, R., M. C. Kennicutt, II, S. T. Sweet, A. V. Milkov, and D. A. DeFreitas (2001), Thermogenic vent gas and gas hydrate in the gulf of Mexico slope: Is gas hydrate decomposition significant?, *Geology*, *29*, 107–110, doi:10.1130/0091-7613(2001)029<0107:TVGAGH>2.0.CO;2.

Snavely, P. D.Jr. (1987), Tertiary geologic framework, neotectonic and petroleum potential of the Oregon-Washington continental margin, in *Geologic and Resource Potential of the Continental Margin of Western North America and Adjacent Ocean Basins—Beaufort Sea to Baja California*, edited by D. W. Scholl, A. Grantz, and J. G. Vedder, pp. 305–351, Circum-Pac. Counc. for Energy and Miner. Resour., Houston, Tex.

Suess, E., et al. (1999), Gas hydrate destabilization: Enhanced dewatering, benthic material turnover and large methane plumes at the Cascadia convergent margin, *Earth Planet. Sci. Lett.*, *170*, 1–15, doi:10.1016/S0012-821X(99)00092-8.

Sultan, N., J. P. Foucher, P. Cochonat, T. Tonnerre, J. F. Bourillet, H. Ondreas, E. Cauquil, and D. Grauls (2004), Dynamics of gas hydrate: Case of the Congo continental slope, *Mar. Geol.*, *206*(1–4), 1–18.

Tarutani, T., R. N. Clayton, and T. K. Meyeda (1969), The effect of polymorphism and magnesium substitution on oxygen isotopic fractionation between calcium carbonate and water, *Geochim. Cosmochim. Acta*, *33*, 987–996, doi:10.1016/0016-7037(69)90108-2.

Teichert, B. M. A., N. Gussone, A. Eisenhauer, and G. Bohrmann (2005a), Clathrites: Archives of near-seafloor pore-fluid evolution ($\delta^{44/40}$Ca, δ^{13}C, δ^{18}O) in gas hydrate environments, *Geology*, *33*, 213–216, doi:10.1130/G21317.1.

Teichert, B. M. A., G. Bohrmann, and E. Suess (2005b), Chemoherms on Hydrate Ridge—Unique microbially mediated carbonate build-ups growing into the water column, *Palaeogeogr. Palaeoclimatol. Palaeoecol.*, *227*, 67–85, doi:10.1016/j.palaeo.2005.04.029.

Tomaru, H., R. Matsumoto, M. E. Torres, and W. S. Borowski (2006), Geological and geochemical constraints on the isotopic composition of interstitial waters from the Hydrate Ridge region, Cascadia Continental Margin [online], *Proc. Ocean Drill. Program Sci. Results, 204*, 20 pp. (Available at http://www-odp.tamu.edu/publications/204_SR/109/109.htm)

Torres, M. E., and M. Kastner (2009), Data report: Clues about carbon cycling in methane bearing sediments using stable isotopes of the dissolved inorganic carbon, IODP Expedition 311 [online], *Proc. Integrated Ocean Drill. Program, 311*, 8 pp., doi:10.2204/iodp.proc.311.206.2009. (Available at http://publications.iodp.org/proceedings/311/206/206_.htm)

Torres, M. E., A. C. Mix, K. Kinports, B. Haley, G. P. Klinkhammer, J. McManus, and M. A. de Angelis (2003), Is methane venting at the seafloor recorded by δ^{13}C of benthic foraminifera shells?, *Paleoceanography*, *18*(3), 1062, doi:10.1029/2002PA000824.

Torres, M. E., B. M. A. Teichert, A. M. Tréhu, W. Borowski, and H. Tomaru (2004), Relationship of pore water freshening to accretionary processes in the Cascadia margin: Fluid sources and gas hydrate abundance, *Geophys. Res. Lett.*, *31*, L22305, doi:10.1029/2004GL021219.

Tréhu, A. M., L. Guibiao, E. Maxwell, and C. Goldfinger (1995), A seismic reflection profile across the Cascadia subduction zone offshore central Oregon: New constraints on methane distribution and crustal structure, *J. Geophys. Res.*, *100*, 15,101–15,116, doi:10.1029/95JB00240.

Tréhu, A. M., P. B. Flemings, N. L. Bangs, J. Chevallier, E. Gràcia, J. E. Johnson, C.-S. Liu, X. Liu, M. Riedel, and M. E. Torres (2004), Feeding methane vents and gas hydrate deposits at south Hydrate Ridge, *Geophys. Res. Lett.*, *31*, L23310, doi:10.1029/2004GL021286.

Tréhu, A. M., M. E. Torres, G. Bohrmann, and F. S. Colwell (2006), Leg 204 synthesis: Gas hydrate distribution and dynamics in the central Cascadia accretionary complex [online], *Proc. Ocean Drill. Program Sci. Results, 204*, 40 pp. (Available at http://www-odp.tamu.edu/publications/204_SR/synth/synth.htm)

Vogt, P. R., and W.-Y. Jung (2002), Holocene mass wasting on upper non-Polar continental slopes—Due to post-Glacial ocean warming and hydrate dissociation?, *Geophys. Res. Lett.*, *29*(9), 1341, doi:10.1029/2001GL013488.

von Huene, R., and I. A. Pecher (1999), Vertical tectonics and the origins of BSRs along the Peru margin, *Earth Planet. Sci. Lett.*, *166*(1–2), 47–55.

von Rad, U., et al. (2000), Gas and fluid venting at the Makran accretionary wedge off Pakistan, *Geo Mar. Lett.*, *20*(1), 10–19.

Xie, X., S. Li, X. Liu, and H. He (2003), Seismic evidence for fluid migration pathways from an overpressured system in the South China Sea, *Geofluids*, *3*(4), 245–253.